Licentiate Thesis
Production Technology
2015 No.1

HÖGSKOLAN VÄST

Laser Welding of Boron Steels for Light-Weight Vehicle Applications

Karl Fahlström

University West
SE-46186 Trollhättan
Sweden
+46 52022 30 00
www.hv.se

ISBN 978-91-87531-04-0

Acknowledgements

The results within this work are a compilation of several projects and studies. The work in these studies has been financed by the member programme "Centre for Joining and Structures (CJS)" at Swerea KIMAB as well as VINNOVA and participating companies of the project "LaserLight". The KK-foundation has been financing the research school of "SiCoMaP".

A special thank is directed towards the people that has been involved in this work in one or another way; Oscar Andersson, Esa Laurila, Glen Hopkins, Arne Melander, Urban Todal, Johnny K Larsson, Janko Banik and the Joining department at Swerea KIMAB.

I would like to gratefully thank my supervisors Lars-Erik Svensson and Leif Karlsson for trying the hopeless task of teaching me to be academic. I would also like to show them and the people close to me my appreciation for their patience with my optimistic time schedule.

Karl Fahlström

Stockholm, 22nd of January 2015

Populärvetenskaplig Sammanfattning

Nyckelord: Lasersvetsning; borstål; höghållfasta stål; hållfasthetsminskning; sprött beteende; sprickrisk; deformationer; lättvikt; kvalitetsproblem

För att kunna möta klimatmål med minskade utsläpp genom minskad bränsleförbrukning så måste dagens fordon bli lättare. Detta kan åstadkommas genom introduktion av nya material med ökad hållfasthet i förhållande till sin vikt. Flera material är lovande, däribland fiberförstärkta kompositer, aluminium, magnesium och höghållfasta stål liksom kombinationer av dessa.

Bland höghållfasta stål är så kallat borstål det mest intressanta materialet. Borstål har hög hållfasthet och styvhet samt är både formbart och svetsbart. Vid tillverkning av bilar så måste borstålet fogas både mot sig själv och mot andra material. Traditionellt sett har motståndspunktsvetsning varit den mest använda metoden, men på senare tid har lasersvetsning blivit mer och mer populärt. Lasersvetsning ger fördelar så som hög produktivitet och ökad styvhet i förbanden.

För att kunna öka användandet av borstål och lasersvetsning inom fordonsindustrin så måste kvalitén hos svetsarna kunna säkerställas. I denna studie har tänkbara problem studerats som kan uppstå vid lasersvetsning av borstål. Även nya varianter av borstål med hållfasthet långt över det traditionella borstålet har inkluderats för att studera möjligheten för ytterligare viktsbesparingar.

Kvalitétsproblemen som studerats är porositet, sprickbildning, oönskad lokal geometri på svetsen, hållfasthetssänkning vid svetsförbandet, samt geometriförändringar på komponenten. Arbetet har inkluderat svetsförsök och analys av egenskaper och deformationer för att kartlägga och förstå inverkan av svetsningen.

Studien har resulterat i ökad kunskap om de vanligt förekommande kvalitétsproblemen. Även rekommendationer för hur dessa problem ska kunna undvikas har tagits fram.

Abstract

Title: Laser Welding of Boron Steels for Light-Weight Vehicle Applications

Keywords: Laser welding; boron steel; high strength steels; strength reduction; brittle behavior; crack susceptibility; distortions; light-weight; quality

ISBN: 978-91-87531-04-0

Laser beam welding has gained a significant interest during the last two decades. The suitability of the process for high volume production has the possibility to give a strong advantage compared to several other welding methods. However, it is important to have the process in full control since various quality issues may otherwise occur. During laser welding of boron steels quality issues such as imperfections, changes in local and global geometry as well as strength reduction can occur. The aspects that need to be considered are strongly depending on alloy content, process parameters etc. These problems that can occur could be fatal for the construction and the lowest level of occurrence is wanted, independent of industry.

The focus of this study has been to investigate the properties of laser welded boron steel. The study includes laser welding of boron alloyed steels with strengths of 1500 MPa and a recently introduced 1900 MPa grade. Focus has been to investigate weldability and the occurrence of cracks, porosity and strength reducing microstructure that can occur during laser welding, as well as distortion studies for tolerances in geometry. The results show that both conventional and 1900 MPa boron alloyed steel are suitable for laser welding. Due to the martensitic structure of welds the material tends to behave brittle. Cracking and porosity do not seem to be an issue limiting the use of these steels. For tolerances in geometry for larger structures tests has been done simulating laser welding of A-pillars and B-pillars. Measurements have been done with Vernier caliper as well as a more advanced optical method capturing the movements during the welding sequence. Results from the tests done on U-shaped beams indicates that depending on the geometry of the structure and heat input distortions can be controlled to give distortions from 1 to 8 mm, at a welding length of 700 mm. This means that important geometry points can be distorted several millimeters if the laser welding process not is controlled.

Appended Publications

Paper A. Laser welding of 1900 MPa boron steel

Peer-reviewed paper presented at "NOLAMP 14 - The 14th Nordic Laser Materials Processing Conference" in Gothenburg, Sweden, August 2013.
Authors: Karl Fahlström[1,2] and Johnny K. Larsson[3]

The laser trials were done by me and Mr. Larsson with help from laser equipment operators at Volvo Cars. The evaluation and writing of the paper was done by me, except the Introduction part that was mainly written by Mr. Larsson.

Paper B. Distortion analysis in laser welding of ultra-high strength steel

Peer-reviewed paper presented at "The sixth Swedish Production Symposium" in Gothenburg, Sweden, September 2014.
Authors: Karl Fahlström[1,2], Oscar Andersson[3,4], Urban Todal[3], Arne Melander[1,4], Lars-Erik Svensson[2] and Leif Karlsson[2]

The laser trials were done by me and Mr. Andersson with help from laser equipment operators at Volvo Cars. Evaluation and writing of the paper was done by me and Mr. Andersson. Mr. Andersson did the modelling and writing of the parts of the paper that considered modelling. I evaluated experiments and wrote the corresponding parts in the paper as well as the Introduction.

Paper C. Minimization of distortions during laser welding of ultra-high strength steel

Peer-reviewed paper presented at "ICALEO – 33rd International congress on applications of lasers & electro-optics" in San Diego, CA USA, October 2014. Accepted for publication in "Journal for Laser Applications (JLA)".
Authors: Karl Fahlström[1,2], Oscar Andersson[3,4], Urban Todal[3] and Arne Melander[1,4]

The laser trials were done by me and Mr. Andersson with help from laser equipment operators at Volvo Cars. Evaluation and writing of the paper was done by me. Mr. Andersson did the modelling and writing of the parts of the paper that considered modelling. I evaluated experiments and wrote the corresponding parts in the paper as well as the Introduction.

[1]Swerea KIMAB AB, Stockholm
[2]University West, Engineering Science, Trollhättan
[3]Volvo Cars Corporation, Gothenburg
[4]XPRES, KTH Royal Institute of Technology, Stockholm

Table of Content

List of abbreviations

Laser = **Light Amplification by Stimulated Emission of Radiation**

LBW = **Laser Beam Welding**

HSS = **High Strength Steel**

UHSS = **Ultra High Strength Steel**

AHSS = **Advanced High Strength Steel**

RSW = **Resistance Spot Welding**

LOM = **Light Optical Microscopy**

HAZ = **Heat Affected Zone**

BIW = **Body-in-White**

CFRP = **Carbon Fiber Reinforced Plastic**

CE = **Carbon Equivalent**

1 Introduction

1.1 Background

Within the transport sector, mainly the automotive industry, lighter weight of vehicles gives several performance benefits such as better handling and acceleration. Despite this, the main driving force for reducing weight would be to reduce energy consumption during use of the vehicle [1-3].

A key enabler for this is material technology, introducing light-weight structures by using low density materials and materials with higher strength to weight ratio i.e. specific strength. Several materials suitable for light-weight design are available today including innovative solutions with laminates of different materials or "hollow" sheet structures. Both the material itself and the use of the material are critical. An important research field within automotive industry is also how to combine different materials within joints, i.e. mixed materials or multi materials. All of this can be considered as light-weight technology [2].

Laser beam welding has been in great focus during the last two decades. Its potential for high volume production has the possibility to give a strong advantage compared to several other welding methods. However, it is important to have the process in full control since quality issues may occur.

This study will investigate laser welding of boron steels. The "Introduction"-chapter will give some basic information regarding ultra-high strength steel (UHSS), lasers, laser beam welding, as well as common quality issues that can occur in laser beam welding.

1.1.1 Ultra-high strength steel

In today's models of road vehicles, e.g. cars, busses and trucks, one can find high strength materials. A widely shared philosophy is to increase the use of high strength material within the structural components of the car to lower the weight and increase the performance. Common components such as front and rear bumper beams, door reinforcements, windscreen upright reinforcements, B-pillar reinforcements, floor and roof reinforcements, and roof and dash panel cross members are historically produced from high strength materials [1-6]. To further reduce the weight of vehicles, both new materials as well as design improvements need to be applied [2, 3].

With high strength materials, unchanged performance with thinner and lighter material is possible. Implementation of ultra-high strength steels incorporates several benefits. Main driving forces are weight reduction, crash performance improvement, high strength and stiffness, cost reduction and sustainability [1-3]. High strength steels (HSS) is available in different grades. According to the X-brand (a cooperative definition of HSS used by Ford of Europe, Volvo Cars, Jaguar and Land Rover) steel material definition HSS are steels with a yield strength higher than 180 MPa [7]. The complete definition of different HSS can be seen in Table 1.

Within the X-brand steel material definition system there are several different classes:

Table 1 – HSS definitions used by Ford of Europe, Volvo Cars, Jaguar and Land Rover.

Steel class	Abbreviation	Min yield strength, MPa
Mild steel/forming grades	MS	< 180
High strength steel	HSS	= 180 < 280
Very high strength steels	VHSS	= 280 < 380
Extra high strength steels	EHSS	= 380 < 800
Ultra high strength steels	UHSS	=> 800

A common steel to use within thin sheet automotive applications are thin sheet dual phase steels (DP-steels). The microstructure of DP-steels consists of a mixture of ferrite and martensite. The martensite is formed as islands within the soft ferritic matrix giving high tensile strength (depending on grade, typical between tensile strength 450-1000 MPa) as well as good elongation and formability [2, 3, 8]. This is considered as the standard steel within the car body, Body-in-White (BIW).

Another type of steel that is increasing in use within the automotive industry is boron steels, the most common grade being 22MnB5. Boron steels are fully martensitic with a typical tensile strength of 1500 MPa. Characteristic properties are high hardness, high stiffness and high tensile strength [1, 2, 9].

Press-hardening, or hot-stamping and die quenching, is a method to produce ultra-high strength components for the automotive industry. The development of this technique has rapidly increased in the last decade [2, 9], and a great advantage is the decrease of spring-back compared to cold forming techniques. Typical components produced by the press-hardening process are structural

parts e.g. A- and B-pillar reinforcements, floor sills, cant rails, side impact door beams and bumper beams.

To enable the boron-alloyed steel material to be formed and further on cooled down to a fully martensitic structure, the material first has to be heated up to its austenitisation temperature at around 880-950°C. To achieve a fully martensitic structure, the cooling rate must exceed 25-30°C/s [1, 2]. The schematic relationship is illustrated in Figure 1. The small amount of boron (~0.002 wt.%) is used to facilitate the quenching process by delay the nucleation of ferrite at the austenite grain boundaries. This will prolong the time until ferrite starts to form during quenching [10].

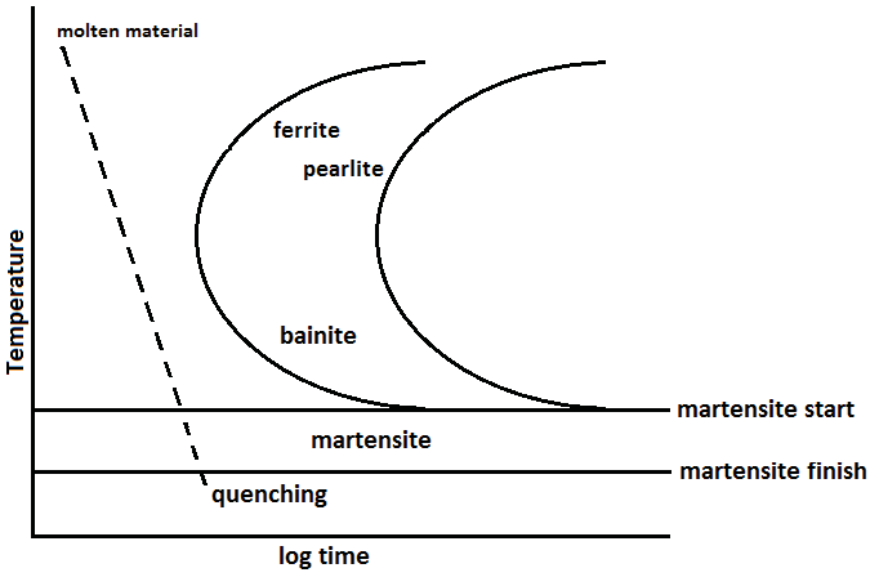

Figure 1 – Illustration of a CCT-diagram (continuous cooling transformation). The martensite is formed through quenching of the steel. Boron delays the nucleation of ferrite in the austenite grain boundaries [10].

To avoid oxidation of the steel during heating and quenching, and to prevent corrosion, it is common to use coating on the steel. A conventional coating consists of a combination of aluminum and silicon (AlSi). Other coating variants are different mixtures of Al, Mg and Zn. Within the automotive industry both uncoated 22MnB5 and AlSi-coated 22MnB5 are common [1, 11].

During the last years new upgraded versions of boron steel have been developed by several steel producers. ThyssenKrupp Steel Europe AG has developed the steel MBW 1900 which contains around 0.34-0.38 wt-% carbon which gives a tensile strength of R_m = 1900 MPa. The carbon equivalent (CE) is approximately 0.57 for MBW 1900 which is higher than for conventional boron

steel (0.47) [12]. SSAB has released Docol 1800 Bor which also is a hardenable boron steel with higher amount of carbon than conventional boron steel, 0.27-0.33 wt-%. With a high cooling rate this gives a tensile strength of R_m = 1845 MPa after water quenching [8].

There is an almost linear relationship between the carbon content, hardness and tensile strength as illustrated in Figure 2 [13]. The higher hardness and tensile strength of these new grades gives further possibilities to produce light-weight components with thin sheet design compared to conventional boron steels [14].

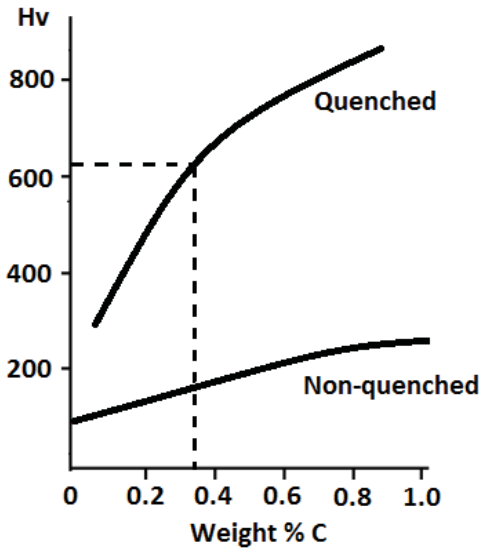

Figure 2 – The relation between the carbon content and hardness of quenched and non-quenched steel [13].

1.1.2 Laser welding

Laser welding is a common joining method within the automotive industry. The method is also used for several other industries such as aerospace, medical, component and construction industry. Traditionally resistance spot welding (RSW) has been the main method used within automotive production. To compete with RSW a new upcoming method has to challenge spot welding within the rather conservative industry regarding production speed, quality assurance, robustness, final properties and running and investment cost. Some of these properties are still of benefit for RSW, but the laser has shown great potential when it comes to production speed, final properties, quality assurance and robustness [3]. To give a greater understanding regarding the potential benefits of the laser process, some background knowledge is given below.

1.1.2.1 Laser as a tool

Laser is an abbreviation of Light Amplification by Stimulated Emission of Radiation. Traditionally CO_2-lasers have been used, but today solid state lasers, such as Disk, Fiber or Diode lasers, are more common within the automotive industry. These have several advantages such as high efficiency and compact design of equipment. Common solid state lasers for laser welding have a wavelength around 1 μm which enables flexible design of equipment where the laser beam is transported through a bendable fiber to the optics focusing the beam at the work piece surface. The optics can be designed in several ways resulting in different focal lengths or beam profiles, used for different purposes.

1.1.2.2 Welding modes

When laser welding, the laser beam is aimed at the materials to be welded causing the materials to melt and fuse together. There are two common welding modes: conduction and keyhole welding. The most common welding mode is keyhole welding. In this case, the laser beam produces a thin but deep vapor cavity, known as a keyhole, in the material. The keyhole occurs by the vaporization of metal. The keyhole remains stable as long as equilibrium exists between vapor pressure and forces due to molten material surrounding the keyhole. The size of the keyhole is approximately the same as the beam diameter, typically 0.6 mm [15]. Keyhole welding is the most common welding mode within the automotive industry.

1.1.2.3 Process parameters

The most important process parameters in laser welding are covered in the following sections. Filler material will not be considered since that is seldom used in laser welding of boron steels.

1.1.2.3.1 Laser power

Conventional laser sources used for laser welding within the automotive industry has around 4-10 kW of power to use. The power is set to create enough penetration in the material. Too much power will cause excessive metal to solidify at the root side of the weld, i.e. dropout welds. Where the parameter window for proper penetration is found is dependent of material, sheet thickness and welding speed. Since high welding speed is wanted, the highest power usually is set and then the welding speed is adapted to get a stable process giving the desired weld profile and penetration. In most cases the power is set close to the upper limit within the parameter window in order to allow for process variations with maintained results [16].

Another aspect of welding power is the delivery mode; both a continuous laser power and pulsed laser power can be used. Pulsed power can be used when heat input should be minimized in order to avoid certain weld defects such as cracking or porosity. However continuous power is better from an efficiency perspective and also the most common delivery mode [16].

1.1.2.3.2 Welding speed

Welding speed is the speed at which the welding process travels. The welding speed [mm/s] is together with laser power [kW] a measure of the heat input [kJ/mm] according to equation 1. Lack of penetration or dropout will occur if welding speed together with power not is optimized [15].

$$Heat\ input\ (Q) = \frac{Laser\ power\ (P)}{travel\ speed\ (v)} \qquad (1)$$

With varying welding speed the weld pool shape and size changes. Lower speeds increases the width of the weld pool and the risk of dropout increases. Higher welding speeds, on the other hand, increases the risk of the weld pool to not have enough time to redistribute to form a smooth joint and will form an undercut instead [16].

1.1.2.3.3 Focus positioning

The focal position relative to the sheet surface has effects on the local shape of the weld and penetration depth. Studies have shown that depending on beam diameter and focal length, the optimum focus position for maximum penetration is approximately 1 mm below the sheet surface for thin sheet applications. The reason is that the heat generation is optimized to generate and maintain the keyhole inside the work piece [15, 17].

1.1.2.3.4 Process gases

In laser beam welding, process gases have three functions; shielding the weld pool, suppression of the plasma and protection of the optics.

The shielding of the weld pool (from both sides of the work piece) may be necessary to prevent oxidation and contamination. Secondly, at high welding power and low welding speeds plasma formation is higher and the excess plasma will defocus the beam and reduce the heat absorbed by the weld. By using a gas jet the plasma can be removed from the critical zone and avoid the unbeneficial effects. Thirdly, weld spatter from the process may damage surrounding equipment especially sensitive glass within the optics. A gas jet can direct the weld spatter in a certain direction and avoid such damages [16-20].

When selecting process gas several parameters must be considered. The most important are plasma suppression ability, density, ionization potential and cost. A common choice is helium, which is optimal in many aspects but may be expensive. Alternative include argon (sometimes combined with small amounts of oxygen or carbon dioxide), nitrogen or pure carbon dioxide depending on application and weld property priority. However, within "non-corrosive" applications, the effect of gas shielding the weld pool is relatively small, and often thin sheet automotive applications are welded without shielding gas [16].

1.1.3 Quality issues in laser welding

During laser welding of common materials for light-weight design (aluminum, magnesium, HSS, etc.), different defects can occur. For a specific component the defects will be considered as quality issues that need to be controlled depending on the level of occurrence. The aspects that need to be considered are strongly depending on material type, main alloying elements, surface condition etc. that are present. Despite this, there are some quality issues that are common for most thin sheet materials while laser welding. These issues are normally considered as critical for the construction and the lowest level of occurrence is wanted, independent of industry.

For thin sheet structures the most critical quality issues can be divided into four categories. These are illustrated in Figure 3.

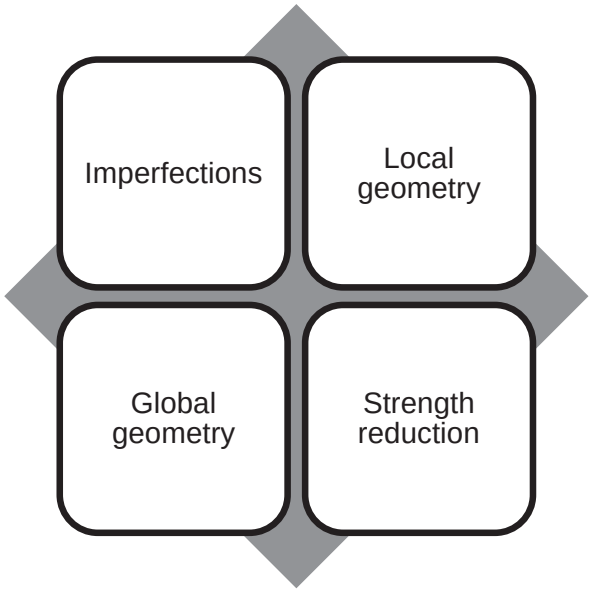

Figure 3 – The four categories of most critical quality issues for thin sheet structures.

Below the common quality issues are described more in detail. As already mentioned, the issues are depending on several factors, and therefore only a generalization will be done to give further background knowledge of phenomena's occurring.

1.1.3.1 Imperfections

Imperfections can be fatal for the joint properties. A small crack or cavity can be the initiation point for a complete failure of the weld in service. When laser welding, the most critical imperfections causing lowered strength are cracks and porosity/cavities.

1.1.3.1.1 Porosities and cavities

Porosity can occur for different reasons. Usually they are caused by instabilities within the keyhole or insufficient shielding gas. Porosity can also be enhanced by contamination or oxides that are vaporized creating gas bubbles that are locked within the melt at solidification. Cavities can occur either by large pores merging or by growth from the interface between the sheets when welding surfaces with high amount of contamination/surface oxide [21].

1.1.3.1.2 Hot cracking

While studying cracks several types that are more common within welding of thin sheet structures has been found. Both solidification cracking and hot cracking refer to the formation of shrinkage cracks during the solidification of weld metal, although hot cracking can also refer to liquation cracking.

Solidification cracks can appear in several locations, and orientations, but most commonly are longitudinal centerline cracks for thin sheet structures. These occur at the intersection where the grains from opposite sides of the weld meet during solidification. Cracking occurs when the available supply of liquid weld metal is insufficient to fill the spaces between solidifying weld metal, which are opened by shrinkage strains [22].

To control solidification cracking, three principal factors need to be controlled: weld metal composition; weld solidification pattern; strain on the solidifying weld metal.

Weld metal composition affects solidification cracking since the composition corresponds to a specific solidification temperature. The weld metal is an invariable alloy with a range of solidification temperatures. Several elements which increase the risk of solidification cracking have been identified such as sulfur and phosphorus. Generally, these are elements which form a second

phase or impurities that get concentrated at the solidification front. The location of these will finally be in the center of the weld which causes sensitivity to weld constraint [22].

In thin sheet applications the weld bead shape dictates the solidification pattern and is influenced largely by welding parameters. Selection of appropriate welding parameters and fit-up give welds which solidify in an upward, rather than inward, direction i.e. those that have a proper width and depth reduces the risk of solidification cracking; but if the pool is too wide, solidification cracking may still occur. It is important to achieve good control over weld shape; a width-to-depth ratio of about 0.5 is usually best for resistance to solidification cracking [22].

1.1.3.1.3 Cold cracking

Ultra high strength steels are quite highly alloyed with carbon to get the proper hardening of the steel during quenching. For conventional boron steel the level of carbon is around 0.24 wt.%, while for boron steels with even higher strength, e.g. MBW 1900 or Docol 1800 Bor, the steel has more than 0.30 wt.% carbon. The CE can be calculated from the following equation (according to IIW recommendations, values in wt.%):

$$CE = + \frac{Mn}{6} + \frac{Cu+Ni}{15} + \frac{Cr+Mo+V}{5} \qquad (2)$$

The CE is used for understanding how the alloying elements affect the hardness of the material. This is then directly related to the risk of hydrogen induced cold cracking. A higher value for the CE is usually related to an increased risk for cracking. Cold cracking, or hydrogen cracking, occurs at lower temperatures, usually below 200°C. The cracks can arise both directly after the welding as well as several hours later. Cold cracks can be found in the heat affected zone (HAZ) and in the weld metal and are promoted by high stresses, a brittle microstructure and hydrogen.

1.1.3.2 Local geometry

Several parameters are influencing the local geometry of the weld. The exterior of the weld can easily be evaluated. Undercut or sunk weld metal depending on improper joint geometry or excess power can be an issue. Although for thin sheet structures the process is quite stable if using proper power. The robustness comes from a small melt pool and rapid cooling when laser welding. Exterior geometry is often a larger problem for fatigue loaded structures (due to crack initiation points created by geometry deviations or defects) of thicker sheets when a larger melt pool is used (e.g. MIG/MAG welding). For crash

components within the automotive industry high static strength and high energy absorption is dimensioning.

An important quality issue that is harder to control is the cross-sectional shape of the weld including the interface between the sheets. Strength of the weld is mainly controlled by the bonded area between the sheets. In an overlap configuration the weld usually gets an hourglass shape resulting in a narrower bonding between the sheets than the sheet interface weld width at the surface. To control the sheet interface weld width at the center, influencing parameters must be understood. In literature it has been found that heat input and focal position are the main parameters influencing the sheet interface weld width [23]. A higher heat input together with a larger spot (caused by defocusing) would give a wider weld in the sheet interface.

1.1.3.3 Global geometry

Components that should be mounted to each other within the assembly line of course need to have the correct dimensions. When exposing material to heat the material expands and when lowering the temperature the material shrinks. If the heat isn't applied homogeneously as in welding, expansion and shrinking occurs differently within the structure. The welding scenario including expansion and shrinkage of welds can result in built in stresses caused when the structure can't move and a distorted geometry [24].

1.1.3.4 Strength reduction

During laser welding of boron steels the fast cooling rate in general creates a hard and brittle martensitic structure in the weld metal and parts of the HAZ where the temperature has reached the upper part of the austenitisation area (where complete austenitisation takes place) [25].

In the HAZ closest to the weld metal the temperature is high enough for complete transformation to austenite, the structure will be completely martensitic after cooling and no softening will take place. In the outmost parts of the HAZ the temperature never exceeds the temperature where transformation to austenite starts [25]. Parts of the HAZ in between these two areas are exposed to temperatures only slightly above the starting temperature for austenite transformation but where transformation is not complete. In these parts, after cooling, some ferrite will remain together with carbides resulting in a zone with lower hardness [25]. Further out some softening will occur due to tempering of the martensite.

Within RSW a too small area of soft material is thought to be the major contributing factor for the sensitivity to the undesired interfacial fracture of

UHSS. For both RSW and laser welding the softer area in the HAZ is called the soft zone and has lower hardness and strength than the weld zone as well as the hard and brittle parts of the HAZ. The soft zone could be wanted, especially within RSW, to control the fracture propagation path [26].

1.2 Research question

Light-weight structures are of great importance for future vehicles. An increased understanding of how to design with and control the properties of new materials and promising joining processes are crucial. This study targets to give further understanding of light-weight design with laser welding of ultra-high strength boron steels. An analysis of the problems that could occur during welding is presented and the boron steels are evaluated.

The overall question to be answered is:

- What laser welding solutions can be developed for boron steels for future light-weight vehicles?

This contains several topics and aspects. To be more specific about the present work, the questions are:

- How does laser welding affect the boron steel in light-weight design?
- What quality problems occur while laser welding?
- Why do the quality problems occur?
- How can these quality problems be avoided?

1.3 Scope

The work done in this study corresponds to a rather strong industrial need of developing robust and flexible manufacturing methods for future light-weight design. It is crucial to develop higher performing, environmental friendly vehicles by using light-weight structures. The academic relevance is to get a greater understanding of laser welding of light-weight materials, such as ultra-high strength steels, and understand the phenomena occurring.

This work is considering boron steel which is considered to be the most promising solution today and is therefore in focus within this study.

Within the projects simulation and FEM-modelling has been used to further understand the phenomena occurring. The work discussed in the thesis is however delimited to the experimental work.

2 Experimental

To consider the different quality issues mentioned in section 1.1.3, different experimental work has been done. Weldability, imperfections and geometry have been hot topics over the years and the methods for evaluation of these are many. The methods used within this work are described below. Studies included are weldability trials of MBW 1900 (Publication: "*Laser welding of 1900 MPa boron steel*") as well as distortions analysis in MBW 1500 (Publications: "*Distortion analysis in laser welding of ultra-high strength steel*" and "*Minimization of distortions during laser welding of ultra-high strength steel*").

2.1 Material

Different trials were done to evaluate the weldability of MBW 1900. Chemical composition and typical properties can be seen in Table 2. In all trials the welded material was in hardened condition. The surface of the steel was blasted to remove surface remnants such as oxides from the hardening process. The steel had no surface coating. Laser welding in hardened condition should illustrate assembly of larger structures in production. Four different material combinations were welded in overlap configuration. The material combinations are shown below.

- 1.0 + 1.0 mm
- 1.0 + 1.5 mm
- 1.5 + 1.0 mm
- 1.5 + 1.5 mm

In the distortion study MBW 1500P with AlSi coating (+AS) was used. Chemical composition and typical properties can be seen in Table 2. The steel was hot formed into a U-beam-geometry which in combination with a flat sheet could be altered into two geometries generating two different distortion modes, see Figure 4. One beam should give possibility to asymmetric deformation when joining a hat-profile with a flat sheet (hereafter named "single hat") of MBW1500P, and the other symmetric deformation along the neutral plane of the geometry when joining two hat-profiles (hereafter named "double hat"). The two cases were chosen as simplified models to simulate A- and B-pillars. The thickness of the material was 1.0 mm and the length of the beam was 700 mm.

Table 2 – The chemical composition and typical properties of MBW 1500 and MBW 1900.

Steel grade	C max	Si max	Mn max	P max	S max	Al min	Nb max	Ti max	Cr+Mo max	B max
MBW 1500	0.25	0.4	1.4	0.025	0.01	0.015	-	0.05	0.5	0.005
MBW 1900	0.38	0.4	1.4	0.025	0.01	0.015	-	0.13	0.5	0.005

	Yield strength $R_{p0.2}$ [MPa]	Tensile strength R_m [MPa]	Elongation A_{80} [%]
MBW 1500	1000	1500	5
MBW 1900	1200	1900	4

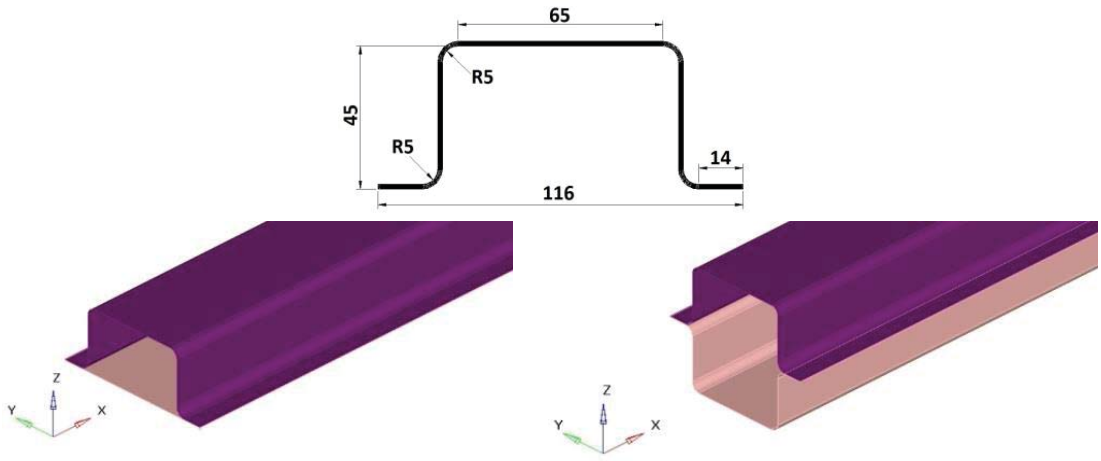

Figure 4 – The cross-sectional dimensions of the hat profile used for distortions studies (upper). Single hat and double hat geometries (lower).

2.2 Welding trials

The welding was done with a HL4006D Nd:YAG laser from Trumpf with Permanova optics (200/200). A 0.6 mm spot diameter with reference focus position on the top surface of the material was used.

For the welding trials in MBW 1900 different parameters was used. These can be seen in Table 3.

Table 3 – The laser welding parameters used for weldability trials in MBW 1900 in four different thickness combinations.

	1.0 + 1.0 mm	1.0 + 1.5 mm	1.5 + 1.0 mm	1.5 + 1.5 mm
Power	3.8 kW	3.8 kW	3.8 kW	3.8 kW
Welding speed	5.5 m/min	5.0 m/min	4.0 m/min	4.5 m/min
Focus position	0	0	+2.5	+1.5

For the distortion studies the power was set to 4.0 kW and the welding speed was set to 1.5, 3.5 and 7.5 m/min. The optics was placed perpendicular to the sheet surface and welding direction. Three scenarios were created only varying the welding speed to create different heat inputs to the material.

The beams were mounted in a robust fixture, shown in Figure 5. The fixture holds the flanges with five 40 mm wide clamps evenly distributed on each flange, using pneumatics. The clamping force was set individually for each clamp. The welding was done at the center of the flange in opposite directions for the two sides, as illustrated by the red arrows in Figure 5. The clamps covered 3 mm of the flange perpendicular to the longer edge.

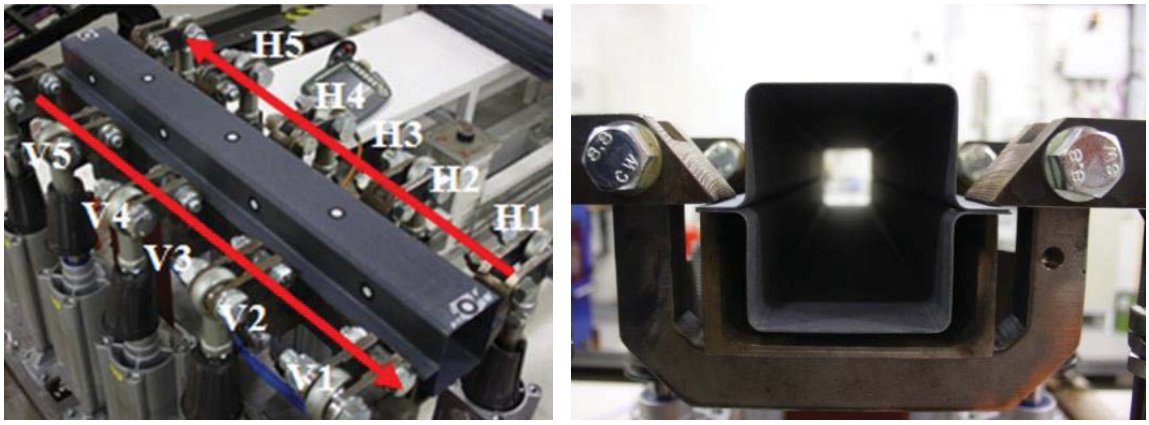

Figure 5 – The fixture used during welding. The fixture holds the beam with 10 clamps, H1 – H5 and V1 – V5.

Within the distortion study the full sequence consisted of welding, cooling for three minutes, and then unclamping with 10 seconds between unclamping each opposite pair of clamps starting from one end. The last clamping pair (H1 + V1) was unclamped after 30 seconds instead of 10 seconds. The welding and unclamping sequence is described in Table 4.

Table 4 – The welding and unclamping sequence used during distortion studies.

Activity:	Time and details:
Welding	11/24/55 sec depending on welding speed
Cooling	180 sec
Unclamping	Pair H5 + V5
Unclamping	Pair H4 + V4 after 10 sec
Unclamping	Pair H3 + V3 after 10 sec
Unclamping	Pair H2 + V2 after 10 sec
Unclamping	Pair H1 + V1 after 30 sec

2.3 Evaluation of local geometry, imperfections and strength

To evaluate the welds in MBW 1900, several tests have been done. For strength determination, shear tensile tests and cross-tension tests were done. In the shear test 48 mm wide and 125 mm long samples were welded with an overlap of 20 mm. The length of the weld seam was 25 mm. For cross-tension tests a 25 mm long weld seam was made as well, but the 125 mm long samples were placed as a cross. See Figure 6.

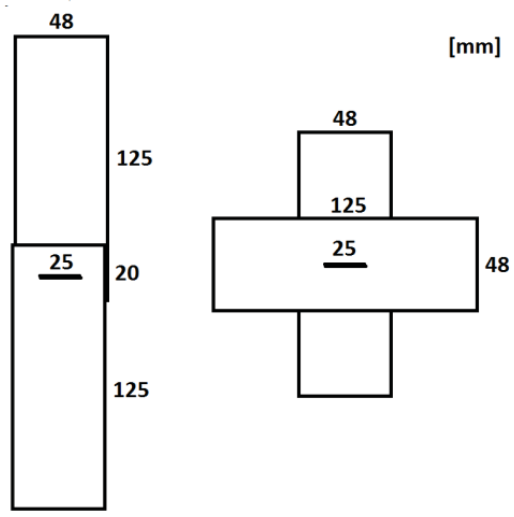

Figure 6 – The dimension of shear tensile and cross-tension test specimens. The weld length used was 25 mm.

The samples were then pulled apart with a speed of 10 mm/min and the force and elongation was measured and plotted. The shear tensile samples were pulled in the length-direction of the sheets, and the cross-tension samples were pulled

in the direction perpendicular to the surface. The tensile testing equipment used was an Instron (100 kN).

Hardness measurements (Vickers) were done on the three different welding speeds samples in MBW 1500. Indentations were done with a load of 0.5 kg. The hardness values were plotted from the center of the weld in the upper sheet. Hardness measurements were also done in the base material.

For detection of imperfections within the weld metal, light optical microscopy (LOM) has been used. Both cracks and porosity can in most cases be seen in LOM. Evaluation has been done on cross-sections taken at representative locations. To have a good image and to see the microstructure, the samples have been polished and etched with Nital (2%).

Cracking can be evaluated with several methods. One part of the new collaborative standard E SEP 1220-3 has been evaluated within this project. With SEP the probability of hot cracking is evaluated by relative studies between different materials. In the test a weld is made 2 mm from one corner of a sample to 15 mm from the second corner; an angled linear weld. This can be seen in Figure 7. This is done as bead on plate with 10 repetitions. A crack is expected to be developed from the corner of the weld closest to the edge since the heat conductivity is restrained by the edge itself. The sample is then broken along the weld seam, and the oxidized length of the weld is measured. This length corresponds to the crack length that is believed to have occurred during welding.

Figure 7 – Specimen used for hot crack susceptibility test according to E SEP 1220-3.

2.4 Global geometry

Two methods were used for evaluation of how much the structure has distorted during the whole sequence of welding, cooling and unclamping has been used. A simple, but effective method is measurement of the component (width and

height) at three reference points (middle and the two ends) before and after the welding sequence.

Another method that has been used is a system called Move Inspect, produced by Aicon 3D Systems. Move Inspect is an optical measurement technology. The system consist of three cameras placed at a distance of approximately 2 m from the geometry to be measured. The system recognizes measurement points (small circular stickers) placed on the component, and record the position with x-, y-, and z- coordinates at a frequency of 1-6 Hz. One great benefit of this method is that the recording can be done dynamically during the whole welding sequence including cooling and unclamping. This will give an understanding of where and when the distoritons occur during the sequence.

Figure 8 – The optical measurement system used for recording of distortions. The system recognizes measurement points (small circular stickers) placed on the component, and record the position with x-, y-, and z- coordinates at a frequency of 1-6 Hz.

2.4.1 Modelling of distortions

To predict distortions modelling was used. An FE model was first generated and simulations were performed using ESI Group's Weld Planner. After that a more advanced thermo-metallurgical-mechanical computational model was developed using ESI Group's Sysweld code. The modelling part of the studies is not included in this work. More information and results can be found in the appended papers.

3 Results

The objective of this work was to find robust solutions for laser welding of candidate materials for use in future light-weight vehicles. Therefore, laser welding of conventional boron steels (R_m=1500 MPa) and very high strength boron steels (R_m=1900 MPa) has been evaluated. Structures simulating components for light-weight vehicles have been welded considering both weld quality and geometry. Several quality issues have been identified and controlled. Weldability including especially cracking issues and brittle behavior, as well as global geometry has been evaluated.

In the following section result from welding trials are presented.

3.1 Imperfections

Different sets of welding parameters were used to find a proper welding scenario. The parameters giving most aesthetical welds with respect to weld bead width and height, root side, external defects and penetration was used. In tests included within this study porosity or cavities has not been seen extensively or notably affecting the strength.

The results from the crack evaluation in MBW 1900 using the method described in "Experimental methods" can be seen in Table 5. Tests have been done for two different material thicknesses; 1.0 mm and 1.5 mm.

Table 5 – The oxidized crack length from hot cracking test according to E SEP 1220-3. The measurements show a large scatter.

	Oxidized crack length (mm)										Average:
1.0 mm	16	6	9	0	4	8	9	7	13	9	8.1
1.5 mm	24	0	29	0	0	21	0	18	0	7	9.9

The results suggest that a 1.5 mm sheet is more sensitive to cracking compared to a 1.0 mm, although a large scatter is noticed.

3.2 Local geometry

The local geometry of a weld can be split into exterior and interior geometry. For the exterior geometry a higher heat input gives a more sunk weld resulting in excess material in the root. This is illustrated in Figure 9.

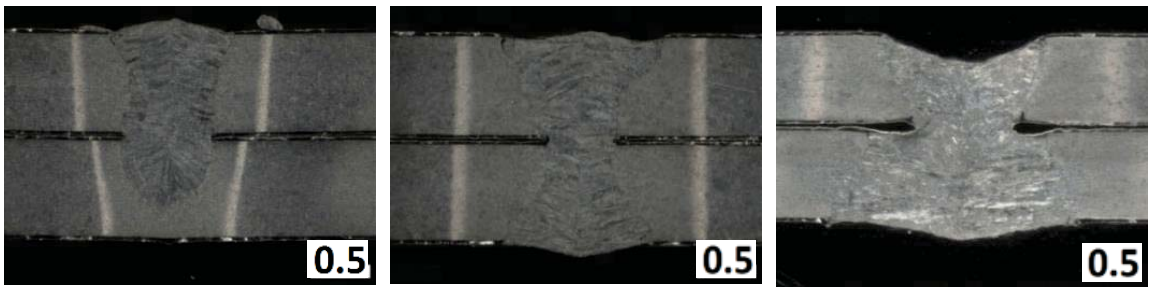

Figure 9 – Cross-sections of MBW 1500 welded with 7.5 m/min (left), 3.5 m/min (middle) and 1.5 m/min (right) welding speed. The scale (0.5) is in mm.

For the interior geometry the main parameter to control in an overlap configuration is the width of the bead at the interface between the sheets. In overlap configuration the weld usually gets an hourglass shape resulting in a narrower bonding between the sheets than the sheet interface weld width at the surface. This is illustrated in Figure 9. It was found that the welding speed, which corresponds to the heat input, affected this width as shown in Figure 10. The results show that the sheet interface weld width using 3.5 m/min is smaller than expected if a linear relationship should occur, but the welding speed of 7.5 m/min only creates partial penetration.

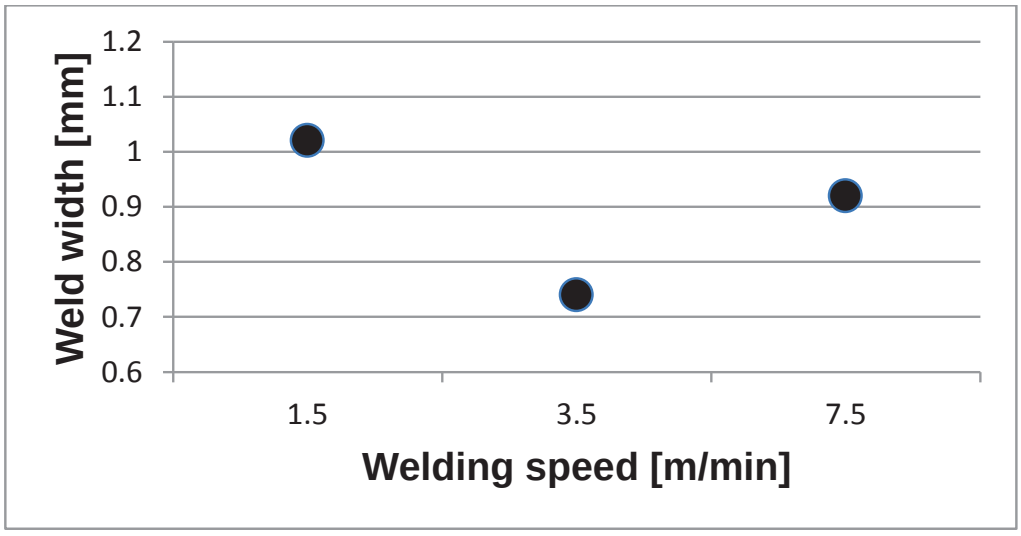

Figure 10 – The relationship between sheet interface weld width and welding speed in MBW 1500.

In welding trials of MBW 1900 the width of the welds in the sheet interface were measured (average of measurements in 3 different cross-sections) for the different thicknesses. The results including heat input are shown in Table 6. The results show that a relatively small sheet interface weld width in relation to the sheet thickness was achieved during welding of 1.5 + 1.5 mm. To keep in mind is the scatter of around ±0.1 mm. The sheet interface weld width corresponds well with the used heat input.

Table 6 - The sheet interface weld width, heat input and the thickness combination of MBW 1900.

Thickness combination [mm]	1.0 + 1.0	1.0 + 1.5	1.5 + 1.0	1.5 + 1.5
Measurement 1	0.75	0.8	1.14	0.87
Measurement 2	0.89	0.87	1.17	1.03
Measurement 3	0.94	0.97	0.98	0.91
Sheet interface average weld width [mm]	0.86	0.88	1.09	0.93
Heat input [kJ/mm]	0.041	0.045	0.057	0.050

Another parameter coupled to the interior geometry is the penetration. Penetration was found to vary with heat input as shown in Figure 9. For tests within MBW 1500, a higher heat input gives a deeper penetration whereas welding with a higher welding speed 7.5 m/min and hence a lower heat input results in partial penetration.

3.3 Global geometry

Within this study measurement of distortions after and during welding has been done. The measurements have been done with Vernier caliper and Move Inspect (described in chapter 2). Components studied are simplified A-pillars (single hat beam) and B-pillars (double hat beam). After being released from the fixture, the single hat beam distortions were small, with a maximum value of around 1.0 mm on a 700 mm weld length. For the double hat beam the distortions were several times larger, with a maximum around 8.0 mm. For the double hat beam it was clear that a higher heat input resulted in a larger distortion. The distortion levels can be seen in Figure 11.

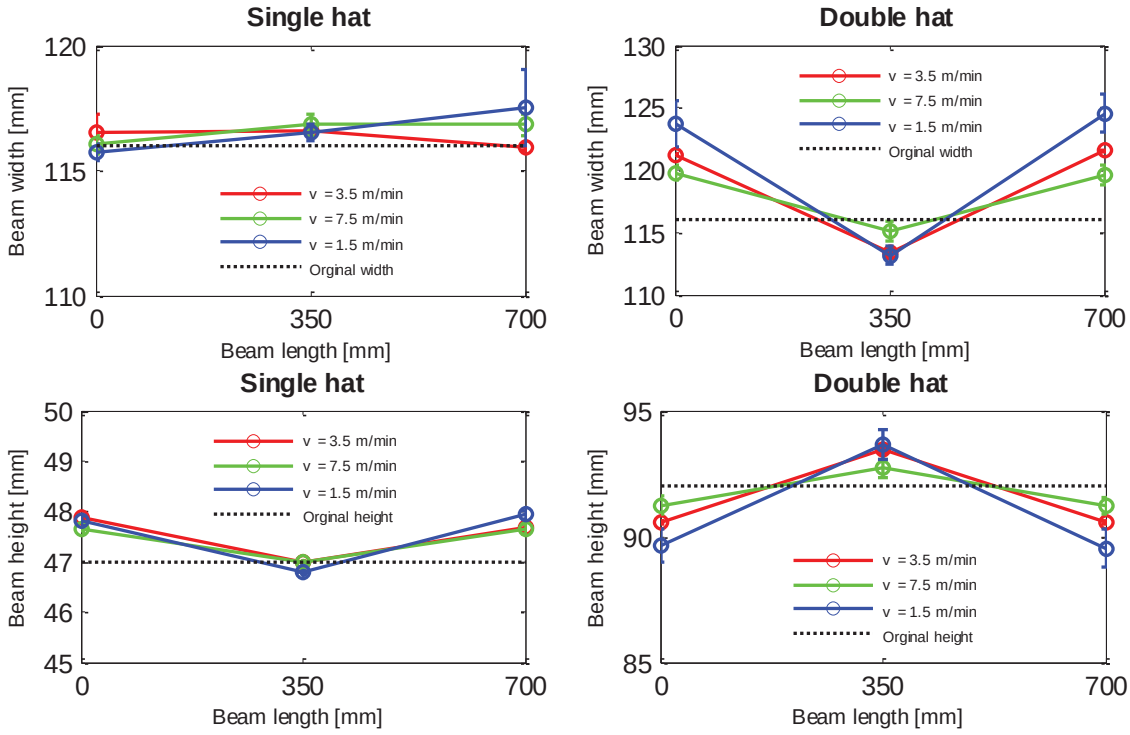

Figure 11 - Showing measurements of the final geometries of the single hat (left) and the double hat (right) done with Vernier caliper. Single hat show distortions around 1.0 mm and double hat show distortions around 8.0 mm.

For measurements with Move Inspect the maximum remaining absolute distortions were in the range of 2 mm for vertical deformation and 1.5 mm for transverse deformation for double hat geometry. This can be seen in Figure 12. Note that the beam was still mounted at one end, e.g. the last clamps were still mounted during recording of the values.

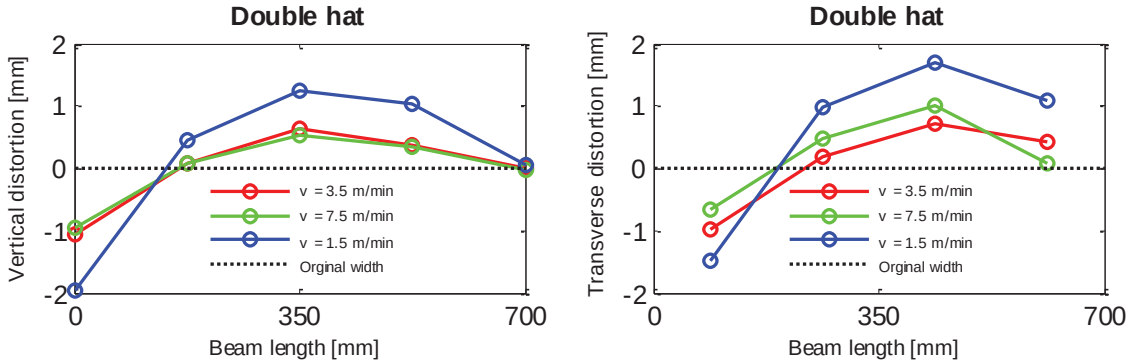

Figure 12 – The measurements done with Move Inspect. The beam is still mounted at 700 mm. Double hat show distortions in the range of 2 mm for vertical deformation and 1.5 mm for transverse deformation.

To understand when the distortions occurred the sequence including welding, cooling and unclamping was recorded with Move Inspect. The total welding time differed since different welding speeds were used. The optical measuring

equipment followed the distortions in all measurement points during welding. As can be seen in Figure 13 quite large deformations occur locally when the laser beam moves during welding (approximately the first 60 s). The different curves in the figure represent different measuring points. After welding the distortions retracted to approximately their initial values due to the strong clamping. During cooling very low distortions were recorded compared to during welding. In this case relatively long cooling time was used to be sure that the distortions not was influenced by cooling during unclamping. When the unclamping began a stepwise increase of distortions arised resulting in the final distorted geometry. An example of measurement of deformation during a complete sequence is illustrated in Figure 13.

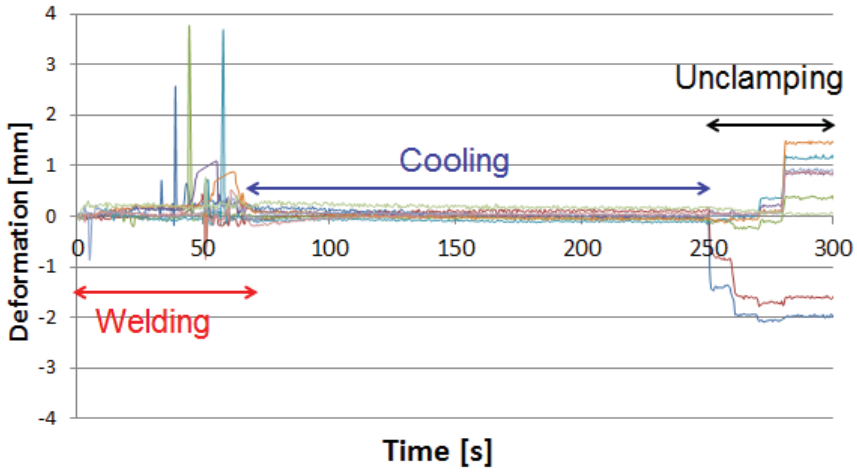

Figure 13 – The movements of measurement points during welding, cooling and unclamping. After welding the distortions retracted to approximately their initial values due to the strong clamping. During cooling very low distortions were recorded compared to during welding. When the unclamping began a stepwise increase of distortions arised resulting in the final distorted geometry.

In general, two different characteristic distortion modes occurred for the two geometries welded, see Figure 14. The single hat beam suffered from transverse shrinkage of the gap between the "legs" of the profile. This resulted in a small height change at the ends of the beam.

The double hat beam suffered from larger distortions than the single hat beam. For double hat, the geometrical change was in the transverse direction with a hourglass looking shape.

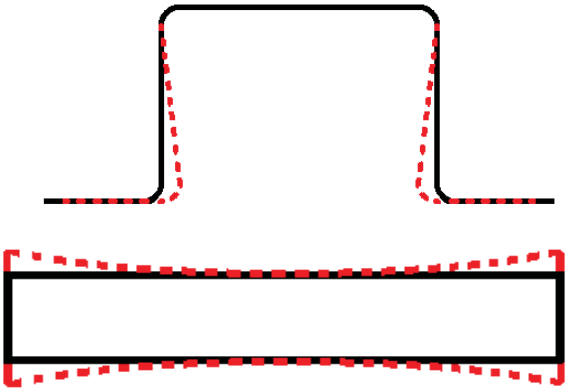

Figure 14 - Two different characteristic distortion modes occurred for the two geometries welded. The single hat beam suffered from transverse shrinkage of the gap between the "legs" of the profile (top). For double hat, the geometrical change was in the transverse direction with an hourglass looking shape (bottom).

3.4 Strength

Results of the tensile testing from laser welding of MBW 1900 are summarized in Table 7 including tensile strength at fracture (F_{max}) and elongation/deflection at fracture (At mm/ε F_{max} mm). The values shown are average values out of 10 samples. A low scatter was obtained. Shear tensile tests were performed within 24 hours as well as after 2 weeks to see if the delayed testing affected the strength. Results show that the strength is within the same range for both tests, although the elongation increases when testing after 2 weeks. Shear strength both after 24h and 2 weeks are higher for 1.5 + 1.0 mm then 1.0 + 1.5 mm. Cross-tension strength and elongation for 1.5 + 1.5 mm are much lower than expected if comparing with cross-tension strength of the other thickness combinations. Thickness combination 1.5 + 1.5 mm was welded with a low heat input, resulting in partial penetration and suffered from an interfacial failure. The other combinations were welded with full penetration and the failure occurred in the border line between outer weld metal and HAZ.

Table 7 – The shear tensile and cross-tension test results. Notice the increase in elongation for tests made after 2 weeks as well as the low cross-tension strength values for 1.5 + 1.5 mm samples.

	Shear, 24h		**Shear, 2 weeks**		**Cross tension**	
	F_{max} kN	At mm	F_{max} kN	At mm	F_{max} kN	ε F_{max} mm
1.0 + 1.0 mm	16.9	4.0	17.8	5.7	3.1	19.5
1.0 + 1.5 mm	20.6	5.2	18.6	5.9	3.7	17.0
1.5 + 1.0 mm	24.8	6.0	23.8	7.6	3.5	18.9
1.5 + 1.5 mm	27.9	5.5	26.5	8.2	0.6	1.6

Hardness measurements were done for the three different welding speeds in MBW 1500. The hardness measurements were done in the center of the upper sheet and are presented in Figure 15. The hardness profiles show that increased heat input gives wider distance between the soft zones as well as a lower hardness of the soft zone. Welding speed 7.5 m/min has a minimum hardness of 330 HV0.5, 3.5 m/min has a minimum of 305 HV0.5, and 1.5 m/min has a minimum of 270 HV0.5. The hardness of the center of the weld metal is close to the base material except for 1.5 m/min. A decrease in hardness can be seen in the outer part of the weld metal for 3.5 and 7.5 m/min. The hardness of the HAZ is highest close to the weld metal. The width of the area between the soft zones is wider than the measured sheet interface weld width. The hardness of the base material was measured to 500 HV0.5 as seen in Table 8.

Table 8 – Hardness of the base material. The values are in HV0.5.

										Average
503	497	501	505	507	497	501	495	498	499	**500**

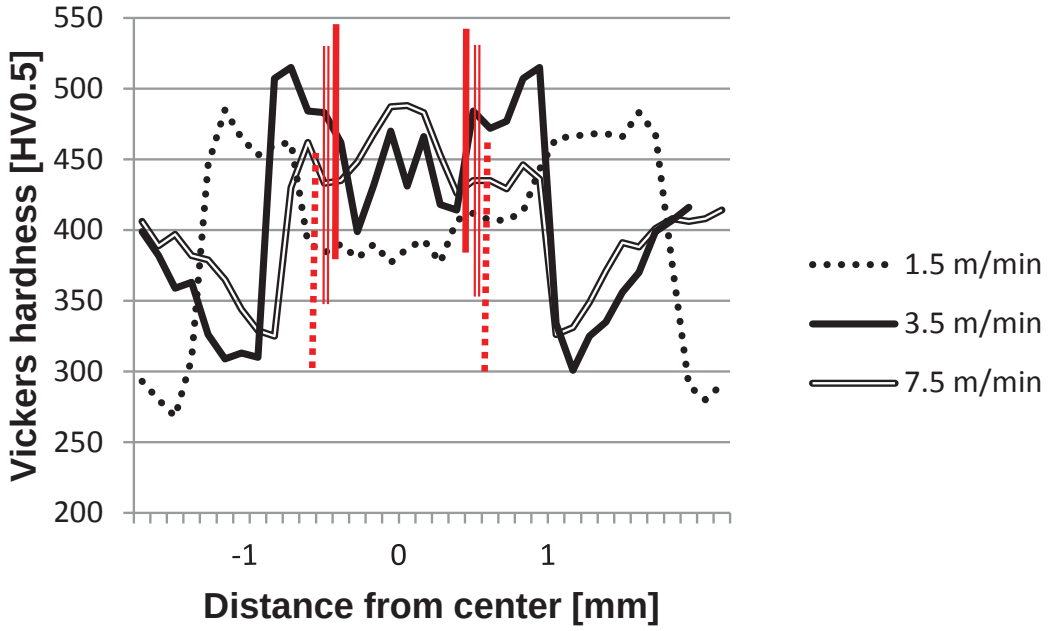

Figure 15 – The hardness (HV0.5) profiles from the three different welding speeds used for MBW 1500 including the weld metal boundary (vertical lines). The hardness profiles are in the centre of the upper sheet. Increased heat input gives wider distance between the soft zones as well as a lower hardness of the soft zone.

4 Discussion

In this work, laser welding of boron steels has been investigated, with respect to distortion and strength of welded joints. A limited study of weldability of a new higher strength version of the boron steel was also conducted. Results are discussed in the following sections.

4.1 Strength

Since boron steels have very high strength, also the welds need to be strong. The rapid cooling after laser welding will give a mainly martensitic weld metal, however a decrease in hardness occur in the outer part of the weld metal when welding MBW 1500 with welding speed 3.5 and 7.5 m/min. For welding speed 1.5 m/min the hardness of the weld metal was around 400 HV0.5. Segregation, annealing during cooling of the weld or a loss of carbon could contribute to the lowered hardness, although the reason for this is not clear.

Martensite has low elongation before fracture and the welds therefore tend to behave brittle during loading. What also occur is that the heat from the laser welding process will give a local softening in the HAZ, see Figure 15. If this soft zone is too wide, the strength of the weld will be lowered.

According to Volvo Cars Corporation guidelines for laser welding the sheet interface weld width should be 0.8 mm to fulfill strength criteria for a sheet stack-up combination with smallest sheet thickness 1.0 mm up to 3.5 mm.

4.1.1 Sheet interface weld width

According to literature heat input, welding speed and focal position are the main parameters influencing the sheet interface weld width [17, 27]. Welding trials in MBW 1500 corresponds to the findings in literature, except for welding speed 7.5 m/min.

The results show that 3.5 m/min welding speed gives a rather small sheet interface weld width (Figure 10). The sheet interface weld width could be increased by increasing the heat input. The reason for the rather large sheet interface weld width during welding with 7.5 m/min could be the partial penetration. Since the heat isn't distributed over the full thickness the width is increasing. However, this must be investigated further.

For welding trials in MBW 1900 the width does not correspond to the stack-up thickness but rather with the heat input used (see Figure 16). In this case full penetration was reached for all thickness combinations except for 1.5 + 1.5 mm. To keep in mind is the difference in focus position (+2.5 mm for 1.5 + 1.0 and +1.5 mm for 1.5 +1.5) presented in "Experimental" which most likely affects the weld width. The laser beam width will increase by defocusing and hence distribute the heat over a larger area causing a wider weld. Therefore, a higher heat input together with a larger spot (caused by defocusing) would give a wider weld in the sheet interface.

However, further sheet interface weld width measurements should be done to validate the correlation.

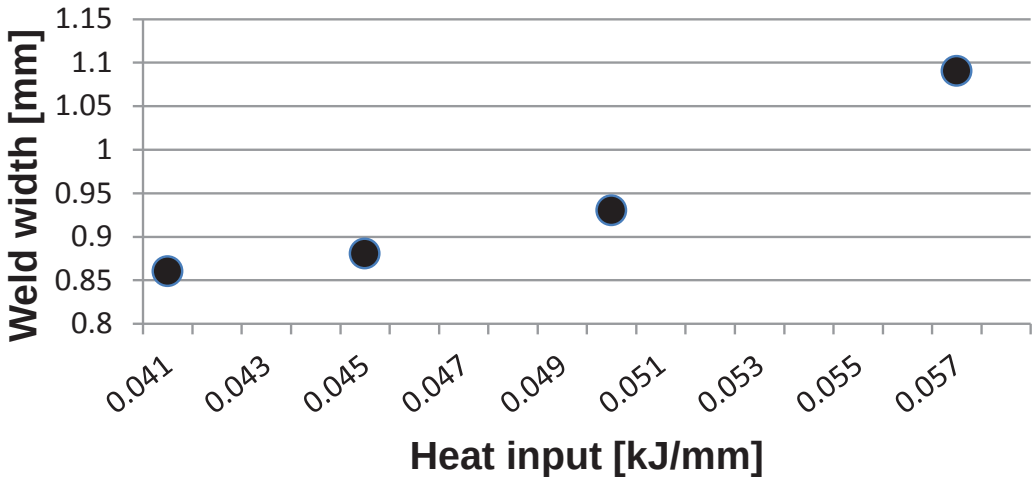

Figure 16 – Relationship between heat input and sheet interface weld width for laser welding trials in MBW 1900.

Approximately 75% of the two sheets get penetrated when welding MBW 1500 in overlap configuration with thickness 1.0 + 1.0 mm, a welding power of 4 kW and a welding speed of 7.5 m/min (see Figure 9). If strength criteria can be reached, this procedure is beneficial from a productivity point of view since lower laser power and higher welding speed can be used.

In a study done by Zhao et al. overlap joints in 0.8 mm DP-steel were welded studying the effect of welding speed on sheet interface weld width [27]. The laser power was kept constant. When the welding speed was increased from 25 to 40 mm/s, sheet interface weld width decreased from 0.64 to 0.47 mm. When the welding speed was 20 mm/s, the sheet interface weld width rose sharply to 1.06 mm. When the welding speed decreased to 15 mm/s, the heat input was too high and the weld pool became violent and unstable. Consequently, obvious variations in sheet interface weld width were observed. These results correspond to the findings in this study, but as mentioned, only for full penetration welds.

Further welding speeds should be tested to more in detail describe the relationship between heat input and sheet interface weld width.

Comparing the shear strength and sheet interface weld width for the different thickness combinations from welding of MBW 1900 (Table 9) shows that 1.0 mm to 1.0 mm results in lower strength than the other. The 1.5 mm to 1.5 mm combination resulted in a relatively high strength. In these tests the strength does not correlate with the sheet interface weld width, rather with the total thickness of the stack-up. The welded area is calculated assuming that the weld is rectangular and hence not considering the half-circular start and stop of the process.

Table 9 – The sheet interface weld width and shear strength of the laser welds in MBW 1900.

	kN	Width	Length	mm^2	MPa
1.0 + 1.0	16.94	0.86	25	21.5	788
1.0 + 1.5	20.60	0.88	25	22.0	936
1.5 + 1.0	24.82	1.09	25	27.25	911
1.5 + 1.5	27.88	0.93	25	23.25	1199

4.1.2 Effects of HAZ softening

During laser welding softening will occur in the HAZ due to the heating. As described in chapter 1, a ferritic soft zone will be present in the HAZ after welding.

If looking at the cross-tension test done in MBW 1900 within this study one can see that the F_{max} in cross-tension tests (Table 7) for combination 1.5 mm to 1.5 mm is low as a result of interfacial fracture. An explanation for this could be that a lower heat input with respect to thickness was used. The lower heat input resulted in a narrow softened area outside the weld metal. As earlier mentioned [26], a too small area of soft material is thought to be the major contributing factor for the sensitivity to the undesired interfacial fracture of UHSS. This suggests that a too wide soft zone would results in an overall low strength, and a too small soft zone will results in a brittle interfacial failure resulting in low cross-tension strength. Further tests needs to be done to verify this and explain the fracture behavior.

Zhao et al. presented that the HAZ of laser welded 22MnB5 is the weakest part of the weld considering shear tensile tests and fatigue [27]. This is confirmed by other authors [25, 28]. It is therefore crucial to control the width of the softened area outside the weld. In Figure 15, hardness profiles are presented for the three different welding speeds. The hardness profiles show that increased heat input gives a larger distance between the soft zones as well as a lower hardness of the

soft zone. However, no clear relationship between the soft zone width (measured at center of upper sheet) and heat input can be seen in this study and must hence be further investigated.

In the study by Zhao et al. it was shown from hardness measurements that a welding speed of 40 mm/s had a lower softening effect compared to a welding speed of 20 mm/s (for a constant laser power) [27]. This is explained to be due to the shorter tempering time in the outer HAZ. The HAZ hardness with welding speed 20 mm/s dropped to 261 HV while with 40 mm/s it only decreased to 350 HV [27]. Furthermore it was shown that a lowered welding speed caused a change of failure mode from interfacial failure to fracture in HAZ during shear tensile tests. If assuming that shear failure mode and cross-tension failure mode is affected in the same way, this supports the hypothesis regarding the failure mode in cross-tension testing of MBW 1900 presented earlier. What should be further investigated is the time and temperature of the different parts of the HAZ during welding and how that affects the hardness and strength.

From the tests it can be seen that tensile strength and fracture mode greatly depended on the weld bead dimension and hardness profile of the weld joint. The summarized hypothesis is that a hard and therefore brittle weld metal in combination with a small sheet interface weld width will result in interfacial failure. The solution to highest strength within laser welds of martensitic steels seems to be to use a proper amount of heat not to cause severe softening of the material, but still avoiding brittle interfacial failures. This is confirmed by Kügler et al. [29].

4.2 Imperfections

Neither cavities nor porosity has been reported to be an issue when welding ultra-high strength steels, if the procedure is adapted properly [27, 28, 30]. During tests done within this study the laser welding process of UHSS show a stable behavior resulting in no visible amounts of pores or cavities.

Conventional boron steels are alloyed and heat treated to give a tensile strength of 1500 MPa. Newer and more advanced steels reach tensile strengths up to 2000 MPa. The reason for the higher strength is a higher carbon content resulting in a higher CE (0.57). A higher CE is expected to result in an increased risk of cold cracking during welding. Tests done within this study did not show any cracking in MBW 1900.

Shear tensile tests were performed within 24 hours as well as after 2 weeks after welding of MBW 1900 to see if the delayed testing affected the strength. Cold

cracks do not always appear directly after welding and hence the delayed testing. The results do not show any lowered strength suggesting that no cracking did occur. However, an increased elongation is seen when shear tensile testing is done after 2 weeks. The increased elongation show that the ductility of the material increases by time with remained strength. A likely reason for this is diffusion of hydrogen, although this needs to be further evaluated.

Hot cracking tests done according to the standard E SEP 1220-3 suggest that the 1.5 mm sheet is more sensitive to cracking compared to a 1.0 mm sheet, although a large scatter is noticed. What could be noticed is that the large scatter and small difference between 1.0 and 1.5 sheet thicknesses give a large uncertainty in the results. What is expected from the testing is that the lower width-to-height ratio of 1.5 mm sheet thickness would cause a higher sensitivity to hot cracking compared to the 1.0 mm sheet due to the more unfavorable solidification pattern. A possible cause of the large scatter in the results is the difficulties in placing the weld seam at the exact same position for each sample. High precision is needed in tenth of millimeters to give the exact same heat distribution within the sheet. The conclusion from these tests is that further testing needs to be done to show the hot crack susceptibility of MBW 1900.

Several laser welding trials were done with different parameters with MBW 1500 and MBW 1900. What has been seen within this study is that both boron steels can be laser welded without cracking with a range of parameters; however both the hot and cold crack susceptibility should be further evaluated.

4.3 Distortions

The welding scenario needs to be controlled since the applied heat from the laser welding causes distortions. It is important to understand the distortions to be able to control them. Within many studies the geometry has been measured after welding [24, 31-35], although when and how the distortions occur within the full sequence is not commonly described. Several articles can be found that describes the final shape of the component, but none has been found that describes the dynamic distortions during laser welding, cooling and unclamping of boron steels.

What can be seen from this work is that the clamping restricts the movement of the beam, creating built-in stresses that cause distortions after unclamping. The methodology of measuring distortions with Move Inspect show great potential for dynamic measurements. The measurements show that distortions occur during welding, but during cooling after welding retract to approximately their initial values (no distortions) due to the strong clamping. The reasons for the initial distortions are probably that the beam is locally heated by the laser and

therefore expands. After laser welding, the temperature of the weld decreases causing shrinkage. Both of these phenomena cause movements of the geometry measurement points. The final geometry of the beam will also depend on the geometry of the cross-section of the beam.

The factor most influencing the distortions seems to be the geometry of the beam. The largest distortion was found for the double-hat profile whereas the single-hat profile exhibited much less distortion. The distortions of the two profiles can be understood as follows: For the double hat the two flanges to be welded are moving away from each other in front of the weld pool during heating. This is due to that expansion occur in the heated solid metal and the center of mass for each profile is located above the flanges (see Figure 17). During cooling the weld shrinks and deformation takes place in the opposite direction, resulting in that the ends of the beam are pressed towards each other resulting in a widening of the cross-sectional geometry (hourglass shape). The symmetry of the cross-section of the beam hinders longitudinal bending and the final geometry will be an hourglass shape.

The single hat profile will mainly deform by longitudinal bending during cooling. This since the cross-sectional geometry is asymmetric (due to a flat sheet) and nothing hinders the longitudinal bending to occur. However, the flat sheet's two-axial locking hinders severe transverse distortion and thereby also decrease the longitudinal bending.

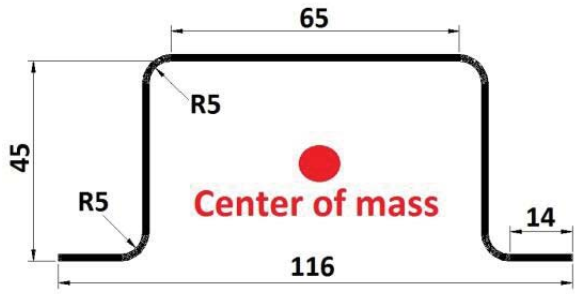

Figure 17 – The approximate center of mass for the hat profile.

If the strength criteria are fulfilled, a partially penetrated weld seems beneficial with respect to the final geometry. Partially penetrated welds show less distortion and have un-molten material in the root of the weld that is believed to decrease distortions. The partially penetrated welds were welded with less heat input which also contributed to less distortion as a higher heat input increased distortions. It is not clear whether the lowered heat input or the partially penetrated weld was the main cause of the lowered distortion.

It is important to find ways to minimize the distortion. Within this study a certain combination of clamping, welding direction and welding pattern was used. What should be further studied is how these influence the final geometry. Intermittent welding would decrease the total amount of heat input which most likely affects the distortions. However, the drawback would be lower strength and stiffness of the structure. In these tests opposite welding directions for the two flanges was used. If parallel welding direction would have been used instead the distortions could also change. Furthermore, the heat should be adjusted to give a stable welding process with suitable penetration. If non-destructive testing can be done to ensure joint quality, partial penetration could be used for further decrease of distortions.

Within production of BIW UHSS is mounted in a framework design and hence welded in hardened condition. If a large fitting issue would be present from distortions of longitudinal welding of flanges, the stiff structure would most likely results in either gap problems or low quality welds. This is a complication as the laser welding process is known to be sensitive to gaps and requires small tolerances [29]. From a practical point of view, laser welded single hat profiles in boron steel could probably be used in a car body, without special precautions. However a flat sheet is most likely not suitable within an A- or B-pillar. Double hat geometry suffered from distortions up to maximum 8.0 mm which most likely is too much from a production point of view.

If distortions cannot be prevented, possibilities exist that could correct a distorted component. What has been used historically within other industry sectors for larger structures that can't be straightened mechanically is counteracting heating. The component is heated locally at certain points to retract to the wanted geometry. The heat releases and creates new internal stresses within the material causing controlled expansion and shrinkage. However, this is not used within the automotive industry and for boron steels this would most likely create a softening effect which makes it less suitable.

Design of critical components that experience a global geometry change during welding could also be adapted to compensate for the distortions or minimize transverse expansion and shrinking as well as longitudinal bending. A first attempt at predicting distortions have been done within the appended papers (Publications: "*Distortion analysis in laser welding of ultra-high strength steel*" and "*Minimization of distortions during laser welding of ultra-high strength steel*"). The simulations give the right shape of the distortions within double hat geometry. However, the models used need further work to give the correct magnitude of distortions.

4.4 Feasibility of laser welded boron steels for light-weight design

4.4.1 Light weight design

The choice of solution for achieving light-weight is not straight forward and the automotive producers seem to aim at different directions. Nevertheless, it is important to understand the importance of light-weight. In a study done by Schubert et al. it is shown that knowing the cost for an existing structure with a certain material it is possible to estimate the savings over the lifetime for the reduced fuel consumption due to the lower weight [36]. For a typical car this value is approximately 9.4 Euro/kg.

There are several materials that are considered as light-weight materials, such as aluminum, magnesium, HSS and CFRP. Carbon fiber reinforced plastics (CFRP) has during the last five years intensively been discussed as a solution for the environmental demands [28]. Also the right material at the right place has been identified to be an enabler. This considers joining technologies for multi material design which is probably the hottest topic within automotive BIW research [9, 28, 37]. In the work presented in this thesis boron steels has been studied.

4.4.2 Laser welding of boron steel

One solution to achieve successful design and production of light-weight vehicles is to use boron steels due to their high strength-to-weight ratio and high stiffness. As a joining technique RSW has been used historically, but laser welding gives further possibilities of increased performance in forms of higher stiffness, as well as a further reduced weight due to possibilities of having smaller flanges.

In a study by Bouaziz et al. HSS is considered to be a promising solution for "lightening", which is referred to as the reduction of weight of a component through the use of a thinner section of a steel with a higher yield or tensile strength [2]. In the conclusions of the study weldability is considered to be one of three technology key areas for future optimizations.

From this study it can be concluded that the sheet interface weld width criteria could be fulfilled for both MBW 1500 and MBW 1900. Considering strength, no cracking or porosity has been found that affects the strength of the weld. As for weld quality no limiting aspects has been found. Boron steels therefore seem suitable for use in BIW applications with the new grade MBW 1900 giving the possibility for thinner gauges and further weight reduction. The largest problem

for utilizing laser welded boron steel seems to be the tendency for large scale distortion. This can however be controlled by the design since the factor influencing distortions most seems to be the geometry of the beam.

5 Conclusions

Laser welding of boron steel for enabling light-weight design has been studied. The study included weldability studies and an investigation of quality issues that could arise. Focus has been on imperfections, distortions and strength reduction. Welding trials has been performed and evaluated with shear and cross-tension testing, cracking susceptibility tests, cross-section studies and distortion measurements.

- Both conventional 1500 MPa boron steels as well as a new 1900 MPa grade can be laser welded successfully with a stable welding process behavior.
- Cracking and porosity do not seem to be an issue limiting the use of these steels.
- The sheet interface weld width, which together with stack-up thickness correlates with strength of the joint, could be increased by increasing the heat input and defocusing.
- Partial penetration welding with enough sheet interface weld width can potentially be used to avoid large distortions and minimize softening in HAZ.
- Distortion during laser welding of thin sheet boron steel was studied for single and double hat beam profiles.
- Dynamic measurements of distortions during laser welding with an optical measurement technique successfully showed when and where distortions occurred during welding.
- The single hat beam suffered from longitudinal bending due to its asymmetric geometry whereas the double hat beam suffered from transverse expansion resulting in an hourglass shape.
- The maximum single hat distortion was around 1.0 mm while the maximum double hat distortion reached 8.0 mm.
- Distortions occur, mainly in the two ends of the beam but retract during welding. During unclamping the distortions increase stepwise with the release of each clamp.

6 Future work

Further knowledge is needed to achieve light-weight design that fulfills the environmental demands of the future. Research needs to be focused on advanced materials, joining methods, properties and design. In this study boron steels has been studied. Future work could include design with other light-weight materials: aluminum, magnesium as well as composites. Joining techniques for such materials should be compared for most successful results.

Several material producers offer boron steels with higher strength than conventional steels. These steels need to be evaluated with respect to weldability. Cold cracking susceptibility should be more extensively evaluated to ensure that the high carbon content does not affect the weldability significantly. Microstructure and hardness profiles should be studied in order to clarify the fracture behavior of welds. In this study a longer elongation is seen when tensile testing after 2 weeks. Further studies are needed to clarify if this can be related to diffusion of hydrogen.

Improved statistics is needed to verify the observed correlations between heat input, sheet interface weld width, softening in HAZ and strength. In this study partial penetration seems beneficial for minimizing distortions. It would be interesting to compare the influence of the un-molten material in the root and the lower heat input.

Distortion studies with a lower height of the hat profile beam should be studied. The lower height could possibly result in a further understanding of how the cross-sectional geometry affects the distortion level and shape. Also more complex geometries should be studied to further learn about how structures will deform. More production like fixtures should be used for further learning. Also, in this study a certain clamping, welding direction and welding pattern was used. What should be further studied is how these influence the final geometry. Intermittent welding would decrease the total amount of heat input which most likely affects the distortions. In these tests opposite welding direction for the two flanges was used. If a parallel welding direction would have been used instead the distortions could change.

Residual stresses should be analyzed to further understand the occurrence of distortions. Also to further couple modelling with experiments to have the possibility to predict distortions should be done.

7 References

1. Jüttner, O.S.M.Z.S., *Determination of hydrogen input in welded joints of press-hardened 22MnB5 steel.* Weld world, 2014(58): p. 339-346.
2. Bouaziz, O., H. Zurob, and M. Huang, *Driving Force and Logic of Development of Advanced High Strength Steels for Automotive Applications.* steel research international, 2013: p. n/a-n/a.
3. Shiquan Zhou, Y.Z., Zhenguo Peng, and Fangjie Ren, *The Investigation of Laser LapWelding Process on High-Strength Galvanized Steel Sheets.* ISRN Mechanical Engineering, 2011. **2011**.
4. Mittal, A., *Steels for hot stamping - USIBOR*. p. Extract from the product catalogue - European edition.
5. Naganathan, L.P.A., *Hot stamping.* Sheet metal forming - Processes and applications, ASM International, 2012.
6. Mittal, A. *Hot stamping with USIBOR1500P*. in *AP&T Advanced hot stamping seminar*. 2010. Detroit.
7. X-brand, *Cross-brand HSS definition of Ford of Europe, Volvo Cars, Jaguar & Land Rover*, 1999-2009.
8. SSAB, *Docol 1800 Bor - Hardenable boron steel for the automotive industry*, 2013.
9. Vollertsen, H.K.F., *Inductive preheating in laser beam welding of multimaterial joints of 22MnB5 and AA6016.* Physics Procedia, 2013(41): p. 41-48.
10. H.K.D.H. Bhadeshia, L.-E.S.a.B.G. *Theory for the formation of Allotriomorphic Ferrite in Steel Weld Deposits*. in *Proceedings of an International Conference on Welding Metallurgy of Structural Steels*. 1987. Warrendale, Pennsylvania: The Metallurgical Society of the AIME.
11. H. Karbasian, A.E.T., *A review on hot stamping.* Journal of Materials Processing Technology, 2010(210): p. 2103–2118.
12. ThyssenKrupp, *Manganese-boron steels MBW*, 2014, ThyssenKrupp Steel Europe AG.
13. Mats Hillert, J.Å., Annika Borgenstam, *Mikro och nanostrukturer i materialdesign*2005, Stockholm: US-AB.
14. Nishibata, T. and N. Kojima, *Effect of quenching rate on hardness and microstructure of hot-stamped steel.* Journal of Alloys and Compounds, 2013. **577**: p. S549-S554.

15. Steen, W.M., *Laser material processing*2003: Springer.
16. Ion, J., *Laser processing of engineering materials: Principles, procedure and industrial application*2005: Butterworth-Heinemann.
17. Lifang Mei, G.C., Xiangzhong Jin, Yi Zhang, Qiang Wu, *Research on laser welding of high-strength galvanized automobile steel sheets.* Optics and Lasers in Engineering, 2009(47): p. 1117-1124.
18. B.G. Chung, S.R., C.H. Lee, *The effect of shielding gas types on CO2 laser tailored blank weldability of low carbon automotive galvanized steel.* Materials Science and Engineering, 1999(A272): p. 357-362.
19. Uwe Reisgen, M.S., Oleg Mokrov, Essam Ahmed∗, *Shielding gas influences on laser weldability of tailored blanks of advanced automotive steels.* Applied Surface Science, 2010(257): p. 1401-1406.
20. Dominique Grevey, P.S., Eugen Cicala, Sorin Ignat, *Gas protection optimization during Nd:YAG laser welding.* Optics & Laser Technology, 2005(37): p. 647-651.
21. Peter Berger, H.H., Thomas Graf, *Understanding Pore Formation in Laser Beam Welding.* Physics Procedia, 2011(12): p. 241-247.
22. TWI. *What is hot cracking (solidification cracking)?* 2014; Available from: http://www.twi-global.com/technical-knowledge/faqs/material-faqs/faq-what-is-hot-cracking-solidification-cracking/.
23. El-Batahgy, A.-M., *Effect of laser welding parameters on fusion zone shape and solidification structure of austenitic stainless steels.* Materials letters, 1997. **32**: p. 155-163.
24. T. Schenk, I.R., M. Kraska and S. Ohnimus, *A study on the influence of clamping on welding distortion.* Computational Materials Science, 2009. **45**(4): p. 999-1005.
25. Farabi, N., et al., *Microstructure and mechanical properties of laser welded DP600 steel joints.* Materials Science and Engineering: A, 2010. **527**(4-5): p. 1215-1222.
26. J. Wahlsten, P.R., M. Linden, J. Hedegård, *Increasing the ductility of RSW joints in UHS steel through parameter adjustments, part 2*, 2011, Swerea KIMAB: Stockholm.
27. Y. Y. Zhao, Y.S.Z.a.W.H., *Effect of welding speed on microstructure, hardness and tensile properties in laser welding of advanced high strength steel.* Science and Technology of Welding and Joining, 2013. **18**(7): p. 581-590.
28. C.-H. Kim, J.-K.C., M.-J. Kang, Y.-D. Park, *A study on the CO2 laser welding characteristics of high strength steel up to 1500 MPa for*

automotive application. Journal of achievements in materials and manufacturing engineering, 2010. **39**(1): p. 79-86.
29. Helge Kügler, A.G., Christoph Mittelstädt, Felix Möller and Thomas Seefeld. *Gap Tolerant Joining of 22MnB5 Steel by Laser Hybrid Welding with Beam Oscillation and Laser Brazing with Two Laser Beams*. in *ICALEO*. 2014. San Diego, CA.
30. Rajashekhar S. Sharma, P.M., *Weldability of advanced high strength steels using an Yb:YAG disk laser.* Journal of Materials Processing Technology, 2011(211): p. 1888-1897.
31. M. Watanabe, K.S., K. Kimura and R. Hoshi, *Effect of Welding Methods and Sequences on the Residual Stress Distribution of Welded Joints.* Japan Welding Society, 1955. **24**: p. 146-153.
32. Satoh, M.W.a.K., *Effect of welding conditions on the shrinkage distortion in welded structure.* Welding journal, 1961: p. 377-384.
33. M. S. Choubi, M.H.a.M.S., *Investigation of the effect of clamping on residual stresses and distortions in butt-welded plates* Scientia Iranica - Transaction B: Mechanical engineering, 2010. **17**: p. 387-394.
34. Rickers, M.A., *The effect of spring restraint on weld distortion in t-joint fillet welds.* 2009.
35. T. Schenk, I.R., M. Kraska and S. Ohnimus, *Influence of clamping on distortion of welded S355 T-joints.* Science and Technology of Welding and Joining, 2009. **14**(4): p. 369-375.
36. E. Schubert, M.K., I. Zerner, C. Walz, G. Sepold, *Light-weight structures produced by laser beam joining for future applications in automobile and aerospace industry.* Journal of Materials Processing Technology, 2001(115): p. 2-8.
37. Kim, C., M.J. Kang, and Y.D. Park, *Laser welding of Al-Si coated hot stamping steel.* Procedia Engineering, 2011. **10**: p. 2226-2231.

8 Summaries of appended papers

8.1 Laser welding of 1900 MPa boron steel

A new category of boron alloyed advanced high strength steel (UHSS) is entering the market since a couple of years which give great potential for use in the automotive industry. The material is highly alloyed with carbon (0.34 wt.%) which is giving a tensile strength of R_m = 1900 MPa. The study aims to evaluate the weldability of this new grade of boron steel.

Laser welding in hardened condition, simulating the use in an assembly line, shows that cracking and other defects can be avoided. A weld quality similar to welded conventional boron steel can be achieved.

8.2 Distortion analysis in laser welding of ultra-high strength steel

When laser welding UHSS sheets, heating and cooling of the material will cause distortions and may cause low joint quality. 700 mm long U-beam structures of 1 mm thick boron steel simulating structural pillars in BIW constructions have been laser welded along the flanges with different welding speeds to investigate distortion formation. Evaluation has been done by measuring the final geometry after welding and unclamping. The results show distortions in the range of 0-8 mm. Coarse FE simulation methods have also been presented which generally predict the distribution of welding distortions.

8.3 Minimization of distortions during laser welding of ultra-high strength steel

U-beam structures of boron steel simulating B-pillars have been laser welded along the flanges. Welding parameters and clamping have been varied to create different welding sequences and heat input generating a range of distortion levels. The distortions have been recorded with an optical measurement system during welding.

The results show that distortions occur mainly transversely and longitudinally along the profile. Variation in heat input show clear correlation with the final geometry and joint quality. Distortions have been measured during the complete welding sequence showing that the distortions first rise but and then retract during welding and increase again during unclamping of the fixture.

Finally, transient FE simulations have been presented which show the deformation behavior of the profiles during the welding and unclamping process.

9 Appended publications

A

Paper A

Laser welding of 1900 MPa boron steel

Karl Fahlström

Johnny K. Larsson

NOLAMP 14
The 14th Nordic Laser Materials Processing Conference
Gothenburg, Sweden, August 2013

LASER WELDING OF 1900 MPA BORON STEEL

K. FAHLSTRÖM[1], J.K. LARSSON[2]
[1]Swerea KIMAB, Stockholm, Sweden. [2]Volvo Cars Corporation, Gothenburg, Sweden.

Abstract

A new category of boron alloyed advanced high strength steel (AHSS) is entering the market since a couple of years which give great potential for the automotive industry. The driving force is lighter structures with thinner material thicknesses. Conventional boron steel used in the automotive industry reaches around 1500 MPa while the new boron steel goes up to 1900 MPa in strength, allowing thinner gauges for the same construction strength properties. To achieve such properties the material is highly alloyed with carbon (0.34 wt%). This is results in that the welding scenario is predicted to be influenced by cracking and other unwanted phenomena's.
Laser welding in hardened condition, simulating assembly line, shows that cracking and other defects can be avoided i.e. welding quality similar to welded conventional boron steel can be achieved.

Keywords: laser welding, boron steel, cracking, 1900 MPa, automotive industry, light weight, AHSS, assembly line

1 Introduction

In the automotive industry there is a continuously on-going struggle to minimize the weight of the vehicles, without hazarding crucial safety requirements, in order to reduce the "carbon footprint" on the environment [1]. Therefore, numerous variants of high strength steels are introduced in the car body, making it possible to down-gauge the different steel components without the renounce of important properties such as strength, stiffness and the ability to absorb high energy at impact situations.

One such material is the advanced high strength (AHS) press-hardened and hot-formed boron-alloyed steel. Apart from a unique process technology, when manufacturing automotive components in this material, it also contains specific alloy elements in order to guarantee a high ultimate strength. The drawback is that due to the alloy content these components become more difficult to weld. At various loading conditions, these welds also present a different behavior to what is common for welds applied in lower strength steel grades [2]. Therefore, the introduction of press-hardened body components not only affects the production conditions, but also the overall performance of the car body structure.

1.1 The Press-Hardening Process

Press-hardening or hot-stamping and die quenching is a method to produce ultra-high strength components for the automotive industry. It has been used since the mid-80's, and typical components produced by the press-hardening process are e.g. A- and B-pillar reinforcements, floor sills, cant rails, side impact door beams and bumper beams. To enable the Boron-alloyed steel material to be formed and further on cooled down to a fully martensitic structure, the material first has to be heated up to its austenitisation temperature at around 880-950°C. To achieve a fully martensitic structure, the cooling rate must exceed 25-30°C/s. The small

amount of Boron (~ 0.002 weight-%) is used to facilitate the quenching process, wherefore the material often is referred to as Boron steel in colloquial terms.

The hot-forming process is mainly divided into two different approaches, the indirect and the direct one, where the direct process is the most commonly used among the automotive OEMs. These two processes offer different advantages for the final application in terms of design versus cost and available choices for surface protection. Making the first forming step(s) by conventional cold forming, the indirect process offers the possibility for more complex geometries and undercut designs before the shaped components are heated, transferred to the furnace and finally hardened (*Figure 1*). This means that two sets of tools are necessary, one for pressing and one for cooling. One advantage however, with this process, is that it offers the possibility to use a conventional zinc-based coating for cathodic corrosion protection.

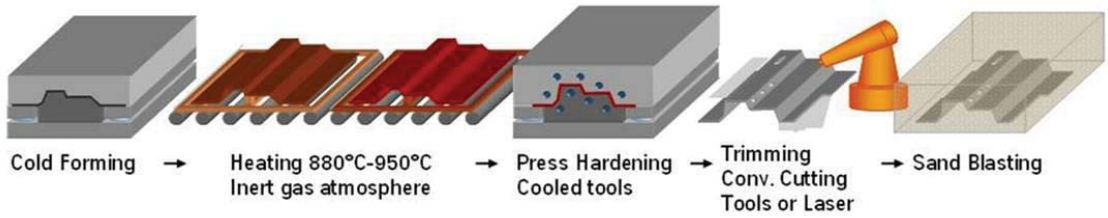

Figure 1. *Schematic description of the indirect hot-forming process with the following steps: cold-forming of the blank in one or several steps, heating of the pressed part to roughly 900°C, rapid cooling of the part to achieve a martensitic structure, post processing like laser- or tool cutting etc.*

In the direct process, the forming operation is integrated with the cooling operation in the same tool (*Figure 2*). This means that the parts reach their final shape and strength in one single press operation, and are therefore often referred to as "hot-stamped" or "hot-formed". The formed components remain in the dies until they have cooled down to between 100-200°C. All Boron-alloyed steel components in today's Volvo cars are manufactured using the direct process [3]. Most car applications such as door beams, bumper beams, sill reinforcements, A-, B- and C-pillars and roof bows can be produced with the direct process. The indirect process might, however, be necessary if more advanced parts are considered.

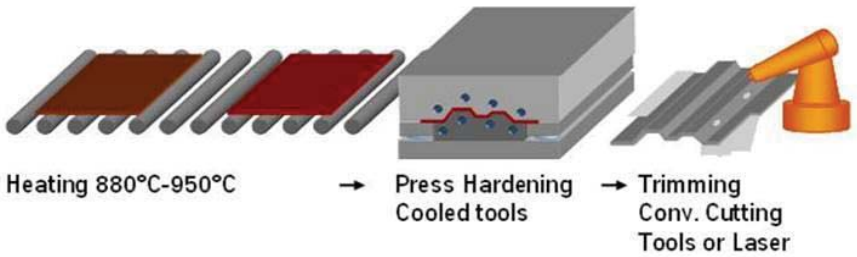

Figure 2. *Schematic description of the direct hot-forming process; heating of the blank to roughly 900°C, pressing of blank to final shape and consequent rapid cooling to achieve a martensitic structure in one single step. post processing like laser- or tool cutting etc.*

The amount of Boron steel in body structures from Volvo Cars has increased from 3% in 2000 to 18% in 2010 [4], and exceeds 20% in conjunction with the launch of the company's latest model - the V40 small estate wagon (*Figure 3*). Fiat, VW and BMW show similar

figures today, but the difference is that today these companies have their own in-house production, whereas Volvo Cars so far purchase all Boron-alloyed parts from external suppliers. The upper limit for Boron steel in a car body is predicted to be around 45%, which more or less includes the whole safety cage with its backing structure. A rough estimation gives that an increase of Boron steel from 10% to 40% would reduce the body weight with approximately 30 kg with unchanged properties, i.e. stiffness, strength, crash and NVH (Noise, Vibrations & Harshness).

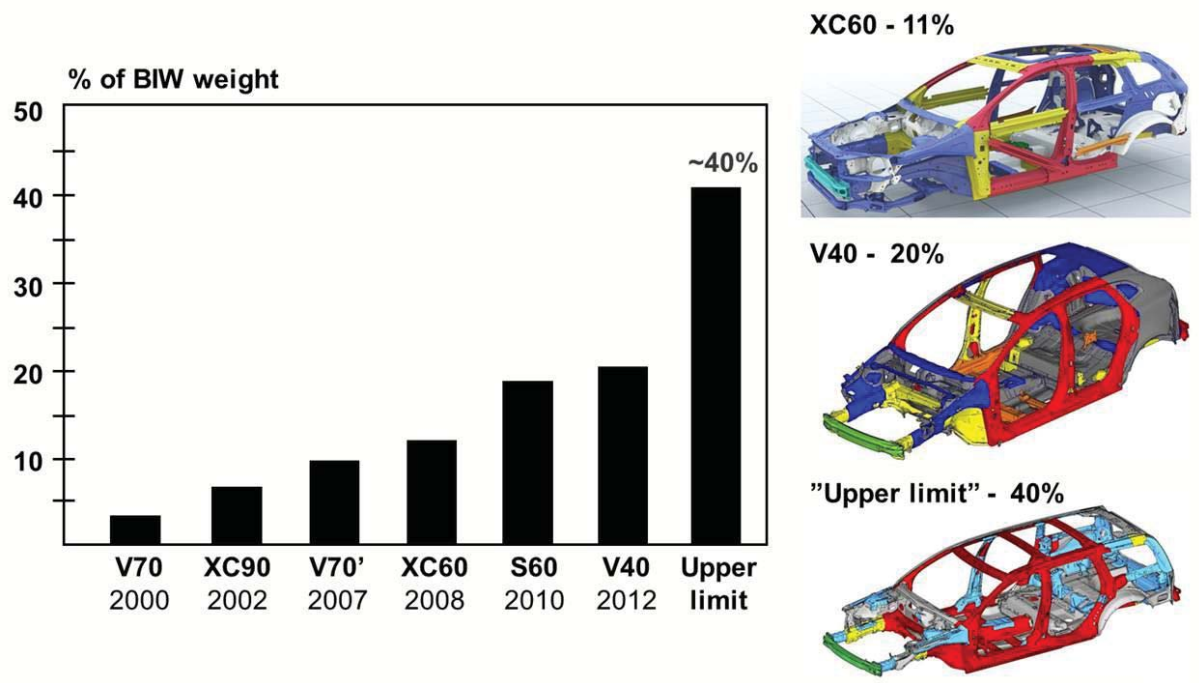

Figure 3. *Development trends regarding the utilization of press-hardened body components at Volvo Car Corporation.*

Laser welding is a common tool for assembly of different components. As described, if thinner and stronger components can be used, further weight savings can be done. This study addresses to investigate the weldability of a new grade of AHSS, MBW-K1900, which is predicted to be influenced by common weld defects due to strength increasing alloy components.

2 Lighter components using thinner material with higher strength

Advanced high strength steels (AHSS) is widely used within the automotive industry, and the usage is expected to increase. AHSS is suitable in front and rear bumper beams, door reinforcements, windscreen upright reinforcements, B-pillar reinforcements, floor and roof reinforcements, and roof and dash panel cross members [5, 6, 7]. The further striving for lighter structures is forcing the automotive producers to use innovative ways to achieve the wanted weight to strength ration of the design. Unchanged performance properties with thinner and lighter material are a critical issue that has been under great focus the past years. Researchers and material producers all over the world is looking for new ways of designing materials that have higher strength but still are suitable for structures in automotive industry. Following objectives are commonly targeted:

- Weight reduction
- Security increasing and crash improvement
- High formability
- Costs reduction
- Sustainability

2.1 MBW-K1900

MBW-K1900 is an AHSS highly alloyed with carbon that is produced by ThyssenKrupp Steel. The extra amount of carbon creates a harder material with higher strength than more conventional boron steels enabling possibilities for thinner gauges. As recognized in the name, MBW-K1900 attains a tensile strength of 1900 MPa. *Table 1* shows the chemical composition of MBW-K1900 and the more conventionally used USIBOR 1500P.

Table 1. *Showing the chemical composition of MBW-K1900 and USIBOR 1500P. The values are in W%.*

	Chemical composition:							
	C	Si	Mn	Al	Cr+Mo	Ti+Nb	B	CE
MBW-K1900	0.343	0.243	0.033	0.033	0.118	0.032	0.0027	0.571
USIBOR 1500P	0.22	0.3	0.032	0.032	0.193	0.039	0.005	0.477

The following equation has been used for calculating the carbon equivalent (CE). The equation corresponds to the IIW-recommendation.

$$CE = \quad + \frac{Mn}{6} + \frac{Cu + Ni}{15} + \frac{Cr + Mo + V}{5}$$

The CE is calculated to be around 0.57 for MBW-K1900 which is higher than for conventional boron steel. It is generally known that the CE should not be higher than approximately 0.5 to expect good weldability, although several other factors need to be considered as well to fully state the weldability. If welding steel with higher CE phenomenon such as hydrogen induced cold cracking can occur. The carbon content also affects the hardness of the material. Measurements done in the bulk of the material show an average hardness of ~600 HV0.5. See *Table 2*.

Table 2. *Showing the Vickers hardness measurement done. 10 measurements were done in the bulk of the material. The average value was calculated.*

Vickers hardness (HV0.5):										Average:
614	622	599	599	625	596	622	617	586	606	**608.8**

In the same way the hardness was measured in the base material before hardening giving an average value of 180 HV0.5. The hardness is strongly connected to the carbon content of the material and the relation is schematically described in *Figure 4*.

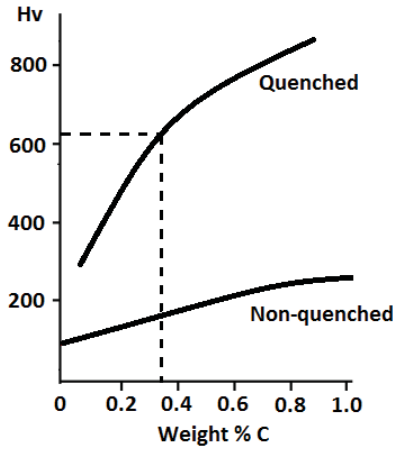

Figure 4. *Schematically showing the hardness–carbon relation for quenched and non-quenched steels.*

The higher hardness and tensile strength is also a result from the quenching cycle. Heating up to austenitising temperature with a following proper quenching will give a fully martensitic structure with wanted properties. How the quenching should be performed is schematically shown in *Figure 5*. The figure illustrates a CCT (continuous cooling transformation) diagram. *Figure 6* is showing the resulting microstructure.

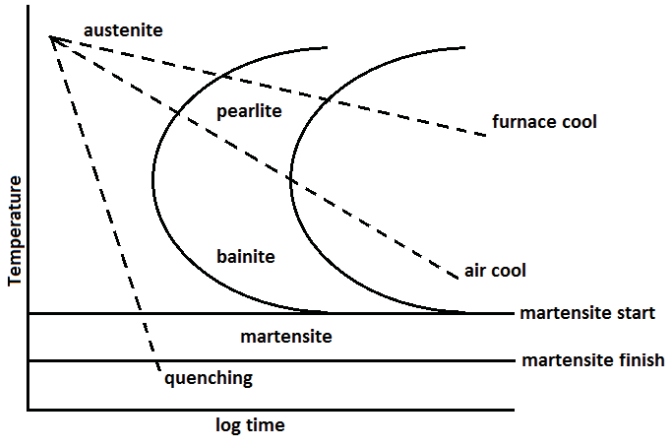

Figure 5. *Showing the CCT diagram for quenching of austenitised steel.*

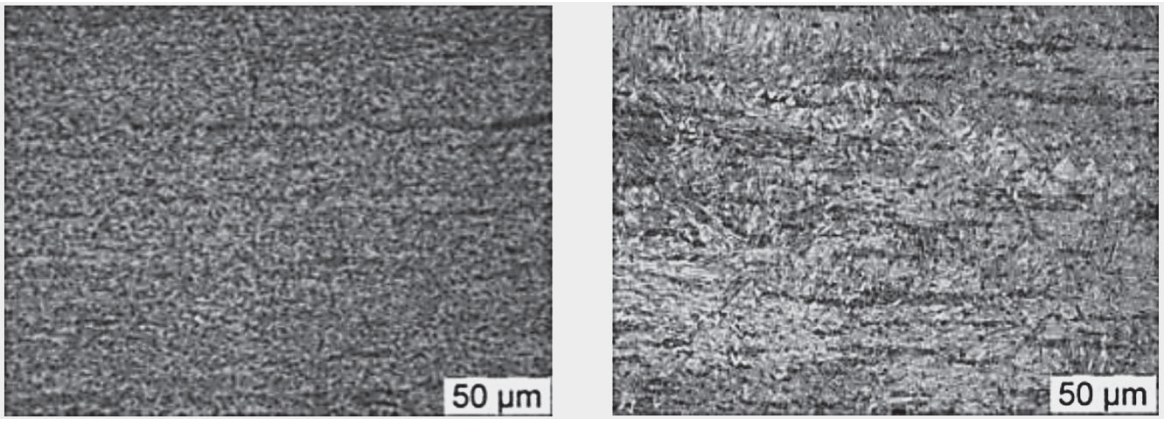

Figure 6. *Left image is showing the microstructure (ferrite-pearlite) for non-quenched steel. The right image is showing the microstructure (fully martensitic) for quenched steel.*

3 EXPERIMENTAL

Different trials were done to evaluate the weldability of MBW-K1900. All trials were welded in hardened condition. The surface of the steel was blasted to remove surface remnants such as oxides from the hardening process. Laser welding in hardened condition should illustrate assembly of larger structures in production.

3.1 Laser welding in hardened condition

Welding trials were performed at Volvo Cars Corporation pilot plant in Torslanda, Sweden. Specifics regarding the equipment and the setup of the trials can be seen in *Figure 7*. The solid state laser was mounted in a robotized motion system.

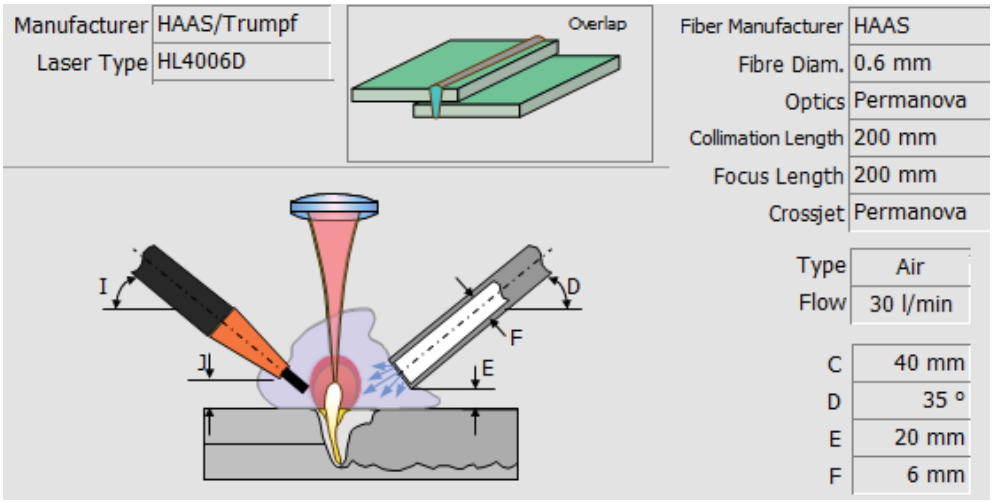

Figure 7. *Showing the setup and the equipment used for laser welding in hardened condition. No filler material was used during these trials. Compressed air was used as shielding of the process.*

The welding was performed on lap joints between the 4 different possible combinations of 1.0 mm and 1.5 mm steel sheets: 1.0 to 1.0, 1.0 to 1.5, 1.5 to 1.0 and 1.5 to 1.5 mm.

Shear tensile tests and cross-tension tests were done. 25 mm weld length on a 48 mm wide coupon was tested at 10 mm/min. Shear tensile tests were performed within 24 hours as well as after 2 weeks to see if cracking occurs after time.

Macrographic images were taken to investigate the weld geometry. Also a crack susceptibility test was performed to investigate the sensitivity for solidification cracking. The test included to weld a seam 2 mm from the corner of a sample to 15 mm from the second corner; an angled linear weld. This is done with bead on plate. After welding the samples were bended along the weld seam to reveal the crack. The oxidized crack length was then measured.

4 RESULTS AND DISCUSSION

4.1 Welding in hardened condition

Different setups of parameters were used to find a proper welding scenario. The parameters giving most aesthetical welds with respect to weld bead width and height, root side, external defects and penetration is shown in *Table 3*.

Table 3. *Showing the parameters giving most aesthetical welds in the different thickness combinations.*

Parameters:	1.0 + 1.0 mm	1.0 + 1.5 mm	1.5 + 1.0 mm	1.5 + 1.5 mm
Power	3800 W	3800 W	3800 W	3800 W
Weld speed	5.5 m/min	5.0 m/min	4.0 m/min	4.5 m/min
Focus position	0	0	2.5	1.5

For respective parameter setup a cross-section image was taken in a light optical microscope to see the internal structure and geometry. All four setups showed nice looking weld geometry with fully martensitic structure and a narrow HAZ. See *Figure 8* to Figure 11.

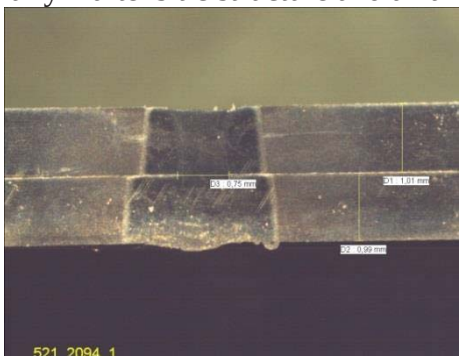

Figure 8. *Showing a macroscopic image of a cross-section in 1.0 mm to 1.0 mm.*

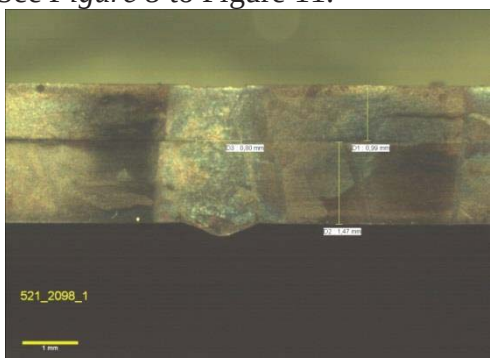

Figure 9. *Showing a macroscopic image of a cross-section in 1.0 mm to 1.5 mm.*

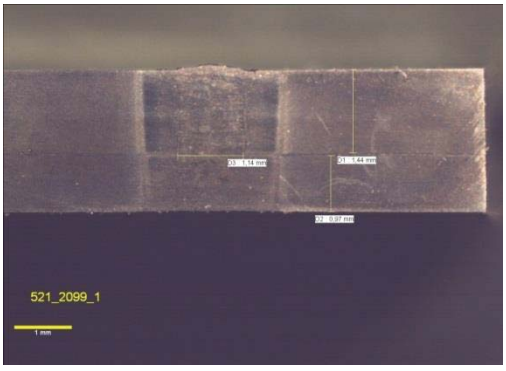

Figure 10. *Showing a macroscopic image of a cross-section in 1.5 mm to 1.0 mm.*

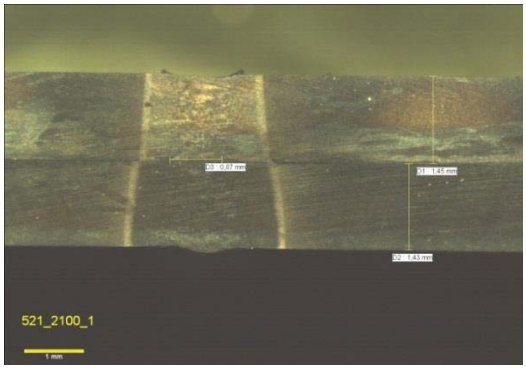

Figure 11. *Showing a macroscopic image of a cross-section in 1.5 mm to 1.5 mm.*

Results of the tensile testing are summarized in *Table 4*. Homogenous values were obtained within each test. Shear tensile tests were performed within 24 hours as well as after 2 weeks to see if cracking occurs after time and therefore causes lower strength. Results show that the strength is within the same range for both tests, although the elongation increases when testing after 2 weeks. The increased elongation show that the ductility of the material increases by time or that softening occurs with remained strength. If looking at the cross-tension test one can see that the F_{max} is as expected for all samples except 1.5 mm to 1.5 mm where a low value was obtained.

Table 4. *Maximum shear and cross-tension strength and elongation at fracture. The values shown are average values out of 10 samples. Fmax (kN) shows the maximum strength, At mm (mm) shows the elongation at fracture, ε Fmax mm (mm) shows the deformation at fracture during cross tension.*

	Shear within 24 h		Shear after 2 weeks		Cross tension	
	Fmax kN	At mm	Fmax kN	At mm	Fmax kN	ε Fmax mm
1.0 + 1.0 mm	16.94	3.97	17.76	5.66	3.07	19.5
1.0 + 1.5 mm	20.6	5.23	18.56	5.87	3.66	17.02
1.5 + 1.0 mm	24.82	5.95	23.75	7.64	3.48	18.86
1.5 + 1.5 mm	27.88	5.49	26.5	8.24	0.61	1.59

Figure 12 shows schematic curves of the shear tensile and cross-tension tests. The behavior of the different samples is the same. The reason for lower cross-tension strength could partly be a consequence of the lower deformation of the sheets seen in *Figure 13* and Figure 14.

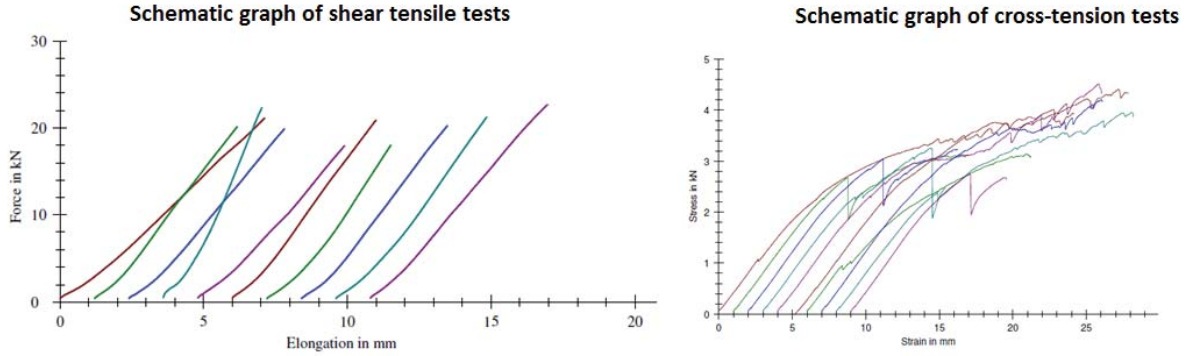

Figure 12. *Illustrating the schematic behavior of the shear tensile tests and the cross-tension tests. Note that the different tests are shifted ~1 mm on the x-axis to clearer show every single specimen.*

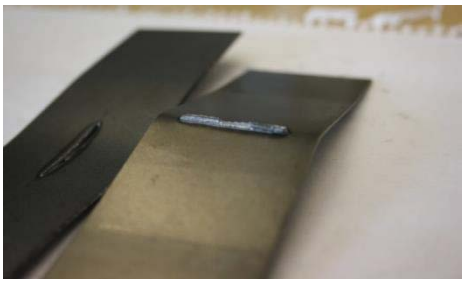

Figure 13. *Showing a deformed 1.0 mm sheet from a cross-tension test. The failure is in the outer weld metal.*

Figure 14. *Showing a non-deformed 1.5 mm sheet from a cross-tension test. The failure is in the interface.*

If looking at the penetration one can see that the penetration depth varies within the different thickness combinations (*Figure 15*). The combination 1.5 to 1.5 mm has less penetration than the other thickness combinations. Also if calculating the heat input per mm thickness of the two joined sheets (a nominal value for the heat input, not dependent on thickness of the sheets) one can see that 1.5 to 1.5 has a lower relative heat inserted to the material (*Table 5*).

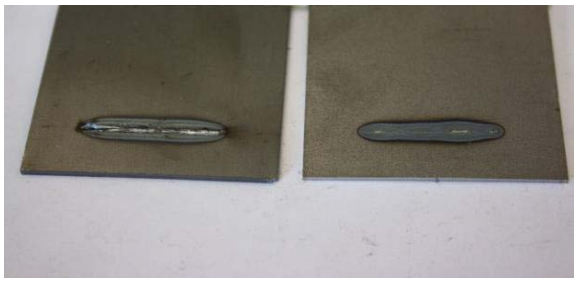

Figure 15. *Showing the not fully penetrated 1.5 mm sheet (left = top, right = bottom).*

Table 5. *Showing the energy inserted to the weld per weld length as well as per mm thickness of the welded sheets.*

	kJ/mm thickness of sheets
1.0 + 1.0 mm	0.0207
1.0 + 1.5 mm	0.0182
1.5 + 1.0 mm	0.0228
1.5 + 1.5 mm	0.0168

4.1.2 Crack susceptibility

One way of examining the crack susceptibility during solidification is to weld a seam 2 mm from the corner of a sample to 15 mm from the second corner; an angled linear weld. This is done with bead on plate. A sample is shown in Figure 16.

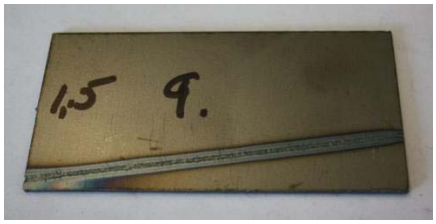

Figure 16. *Showing the angled weld seam of the crack susceptibility test.*

Figure 17. *Showing the bended sample. The bend is done along the seam showing the oxidized length of the crack.*

A crack is expected to be developed from the corner of the weld closest to the edge since the heat conductivity is restrained by the edge itself. The sample is then broken along the weld seam, and the oxidized length of the weld is measured. This length corresponds to the crack length created during the welding sequence. The results from the evaluation can be seen in *Table 6*. The results show that the thicker is more sensitive to cracking. A large spread is noticed indicating the difficulties placing the weld seam at the exact same position for each sample.

Table 6. *Showing the results from the crack susceptibility test. A large spread is noticed indicating the difficulties placing the weld seam at the exact same position for each sample.*

	Oxidized crack length (mm)										Average:
1.0 mm	16	6	9	0	4	8	9	7	13	9	**8.1**
1.5 mm	24	0	29	0	0	21	0	18	0	7	**9.9**

5 CONCLUSIONS

To achieve lighter components within the automotive industry, thinner gauges with higher strength needs to be implemented. A new grade from ThyssenKrupp Steel, MBW-K1900, gives more beneficial strength to weight ratio than more conventional boron steel. The study presented investigates the weldability of this new grade in hardened condition in combinations 1.0 to 1.0, 1.0 to 1.5, 1.5 to 1.0 and 1.5 to 1.5 mm in a lap joint. Laser welding

trials has been performed showing stable process behavior and strength values between 17 and 28 kN for the 25 mm long welds. Low cross tension strength is shown in 1.5 mm to 1.5 mm joints. This is most likely due to that a lower relative heat is inserted into the material. Also crack susceptibility tests was done showing that thicker material is more prone to solidification cracking, although the results show large scattering.

6 ACKNOWLEDGEMENTS

Special thanks to Volvo Cars Corporation for making the welding trials, ThyssenKrupp Steel for material supply and the project group within "Centre for Joining and Structures" for participation in discussions and funding of the project.

7 REFERENCES

[1] Larsson, J.K.:
High Quality Welding of Weight Optimized Passenger Car Bodies – an Important Enabler for Producing Fuel Efficient and Environmental Friendly Products, Proceedings Nordic Welding Conference, Stockholm, Sweden, October 2010

[2] Larsson, J.K.:
Optimizing the Resistance Spot Welding Process for High Quality Welding of Press-Hardened Automotive Components, Proceedings EUROJOIN 8, Pula, Croatia, May 2012

[3] Larsson, J.K., Lundgren, J, Asbjörnsson, E. and Andersson, H.:
Extensive Introduction of Ultra High Strength Steels sets New Standards for Welding in the Body Shop, Proceedings 61st Annual Assembly of the International Institute of Welding (IIW), Joint Workshop Commission III & SC-Auto, Graz, Austria, July 2008

[4] Fermér, M., Jergeus, J., Johansson, R. and Larsson, J. K.:
Hot-Formed Steel in Car Body Structures, International Automotive Body Conference (IABC), Munich, Germany, September 2010

[5] Arcelor Mittal:
Steels for hot stamping - USIBOR®, Extract from the product catalogue – European edition.

[6] Arcelor Mittal
Hot stamping with USIBOR1500P®, AP&T Advanced hot stamping seminar, Detroit, September 15, 2010

[7] A. Naganathan, L. Penter
Hot stamping, Sheet metal forming – Processes and applications, ASM international, 2012

B

Paper B

Distortion analysis in laser welding of ultra-high strength steel

Karl Fahlström

Oscar Andersson

Urban Todal

Arne Melander

Lars-Erik Svensson

Leif Karlsson

The sixth Swedish Production Symposium
Gothenburg, Sweden, September 2014

DISTORTION ANALYSIS IN LASER WELDING OF ULTRA HIGH STRENGTH STEEL

Karl Fahlström[1,2], Oscar Andersson[3,4], Urban Todal[3], Arne Melander[1,4], Lars-Erik Svensson[2], Leif Karlsson[2]

Swerea KIMAB[1], University West, Engineering Science[2], Volvo Cars Corporation[3], XPRES, KTH Royal Institute of Technology[4]

karl.fahlstrom@swerea.se

Abstract: Due to increased demands on reduced weight in automotive industries, the use of ultra high strength steels (UHSS) has increased. When laser welding UHSS sheets, heating and cooling of the material will cause geometrical distortions and may cause low joint quality. 700 mm long U-beam structures of 1 mm thick boron steel simulating structural pillars in body-in-white constructions have been laser welded along the flanges with different welding speeds to investigate distortions and weld quality. The results show that final distortions appear in the range of 0-8 mm. FE simulation methods have also been presented which generally predict the distribution of welding distortions.

Keywords: Laser welding, distortion, UHSS, simulation, automotive

1. INTRODUCTION

1.1 Background

Light weight has been in focus for the automotive industry during several years. Driving forces are lower emissions, reduced energy use and increased performance. Numerous variants of high strength steels have been introduced in the car body, making thinner structures possible without renouncing important properties such as strength, stiffness and the ability to absorb high energy at impact situations.

Ultra-high strength (UHSS) press-hardened and hot-formed boron-alloyed steel is commonly used by automotive industry as a mean of reducing weight and increase crash performance. Apart from the unique process technology during forming, it also contains specific alloy elements in order to guarantee a high ultimate strength. During welding of high strength press-hardened body components, weld quality is important and can be difficult to assure. In addition, due to difficult post-welding straightening of the material, welding distortions are important to keep low. In Figure 1 the trend of increasing use of boron steels can be seen from Volvo Cars Corporation.

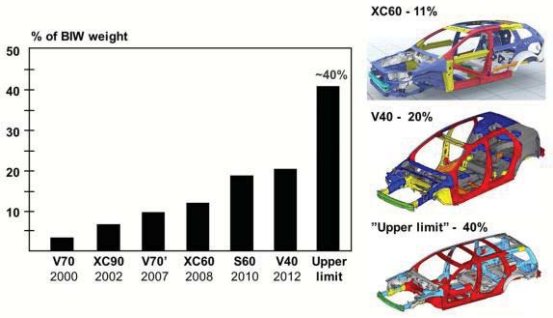

Figure 1 Development trends regarding the utilization of press-hardened body components at Volvo Car Corporation (Fahlström and Larsson, 2013).

UHSS is suitable in several applications within the automotive industry such as front and rear bumper beams, door reinforcements, windscreen upright reinforcements, B-pillar reinforcements, floor and roof reinforcements, and roof and dash panel cross members (Arcelor Mittal, 2010). The further striving for lighter structures is forcing the automotive producers to use innovative ways to achieve the wanted weight to strength ratio of the design. Unchanged performance properties with thinner and lighter material are a critical issue that has been under great focus the past years. Researchers and material producers all over the world are looking for new ways of designing materials that have higher strength but still are suitable for structures in automotive industry. Objectives like weight reduction, safety and crashworthiness, high formability, cost reduction and sustainable are targeted (Fahlström and Larsson, 2013).

A common method for joining these materials is laser welding. Laser welding can be described as a high productivity welding method suitable, with respect to general welding speed and strength properties, for UHSS as well as most automotive applications. The method is usually a compliment to resistance spot welding (RSW) which historically has been the most used method for joining for body-in-white applications due to its low cost and high ability of automation. Laser welding is associated with low heat input but also high cooling rates which strongly affects the material being welded. In addition, laser welding, as opposed to RSW, creates a narrow and continuous weld which is associated with high strength. (Fahlström and Larsson, 2013).

Due to the introduction of heat into the material and asymmetrical structures, welding will cause expansion and shrinkage to result in unwanted remaining geometry changes in the design. It is necessary to control distortions and minimize residual stresses in the material, or ensure that the design compensates them. If not, geometrically important points for assembly can be displaced several millimeters resulting in gaps and low product quality.

Several methods for prediction of welding distortions have been presented. Early research focused on empirical and simplified local models to predict distortions of idealized geometries (Verhaeghe, 1999). While such models were helpful for practical engineers they were often too simplistic to accurately predict distortions in many applications. During the last decades research on prediction of welding distortions has focused on numerical methods and Finite Element (FE) models in particular (Lindgren, 2001). Many papers model the welding process in a thermo-mechanical transient simulation, where the laser beam is modeled as a conductive heat source. However, in order to reduce computation times and pre-processing efforts, research has also focused on simplified FE models where the heat source is approximated as a temperature gradient, which causes displacements due to pure thermal contraction strains. Early studies (Bachorski, et al., 1999) investigated the technique for gas metal arc welding of 6 mm plain carbon steel sheets and concluded that the magnitude of distortions can be accurately predicted. Another study (Tikhomirov, et al., 2005) compared different simulation techniques to predict MAG-welding distortions of an industrial steel control arm in a T-joint configuration. It was concluded that the simplified technique greatly reduced computations times and with proper calibration could predict distortions with good quantitative agreement. A third study (Camilleri, et al., 2006) evaluated the temperature gradient simulation technique on 6 mm fillet welded of a steel with a yield strength of approximately 220 MPa at ambient temperature. Again, the significantly reduced computation times were stressed and the predictions were concluded to be reasonbly accurate.

The present study treats laser welding of thin UHSS sheets in overlap welding. Thus, several process conditions, which have not been investigated by simplified simulations before are introduced. This work will further examine the capacity and range of simplified simulations of welding distortions.

1.2 Aim of paper

The aim of this paper is to investigate where, and to what extent and form, distortions occur while laser welding press-hardened boron steel. Different welding speeds will be used to see the influence of heat input. Welding will be done on hat profile beams simulating A-pillars and B-pillars in automotive structures. The paper aims to assess the predictive capability of a simplified and time efficient FE model for distortions of thin UHSS beam structures after welding and unclamping.

2. EXPERIMENTAL METHODS

2.1 Material

In the present study MBW 1500P steel with AlSi coating (+AS) was used, delivered from ThyssenKrupp Steel. The steel was hot formed into a beam-geometry which in combination with a flat sheet could be altered into two geometries generating two different distortion modes. One beam should give possibility to asymmetric deformation when joining a hat-profile with a flat sheet (hereafter named “single hat”), and the other symmetric deformation along the neutral plane of the geometry when joining two hat-profiles (hereafter named “double hat”), see Figure 2. The two cases were chosen as simplified models to simulate A- and B-pillars. Detailed geometry of the hat profile can be seen in the right figure in Figure 3. Thickness of the material was 1.0 mm and a beam length of 700 mm.

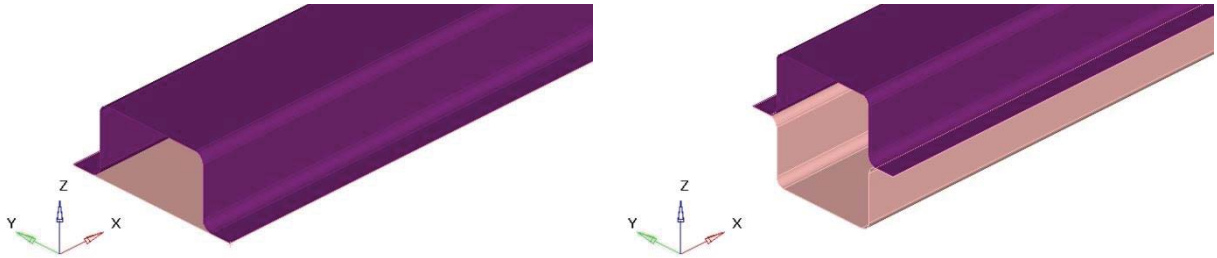

Figure 2 Geometries chosen as type cases, single hat (left) and double hat (right).

2.2 Fixture and welding sequence

The beam was mounted in a robust fixture. The fixture holds the flanges with 5 clamps evenly distributed on each flange, using pneumatics. Clamping force was set individually for each clamp. The welding was done at the center of the flange in opposite directions for the two sides. The clamping range was 3 mm in from the flange edge. The full sequence consisted of welding, cooling for three minutes, and then unclamping with 10 seconds between unclamping each pair of clamps starting from one end. The last clamping pair (H1 + V1) was unclamped after 30 seconds instead of 10 seconds. The sequence is illustrated in Table 1.

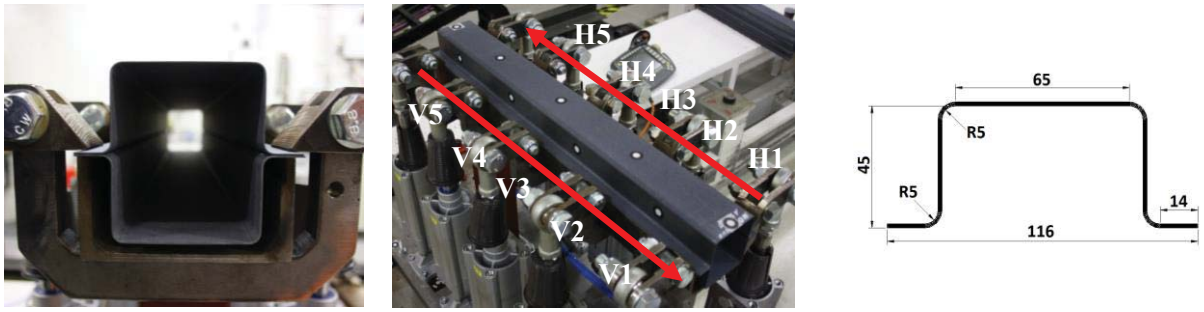

Figure 3 Left and middle picture shows the fixture used during welding trials. In the middle picture the welding direction on each flange can be seen including each clamping H1-H5 and V1-V5. In the right picture the dimensions of the 700 mm long beam are shown in detail (shown in mm).

Table 1 Describing the welding and unclamping sequence.

Welding during 11/24/55 sec depending on welding speed	Cooling during 180 sec	Unclamping pair H5 + V5	Unclamping pair H4 + V4 after 10 sec	Unclamping pair H3 + V3 after 10 sec	Unclamping pair H2 + V2 after 10 sec	Unclamping pair H1 + V1 after 30 sec

The pneumatic clamping was set on 4 bars to ensure sufficient force holding the beams. A lower clamping pressure resulted in separation of the sheets at the faying surface and the gap caused cutting effects from the laser beam. Parameters from the laser welding process can be seen in Table 2. Three setups were used only varying the welding speed to create different heat inputs to the material.

Table 2 Parameters used during laser welding.

Welding speed (m/min)	**Power (W)**	**Focal position**	**Spot size (µm)**	**Laser source**	**Optics**	**Travel angle**
1.5	4000	Surface	600	HL4006D	Permanova 200/200	0º
3.5	4000	Surface	600	HL4006D	Permanova 200/200	0º
7.5	4000	Surface	600	HL4006D	Permanova 200/200	0º

2.4 Measurement of distortions

After the welding sequence, cooling and unclamping the beam geometry was measured. The total height and width of the beam was measured at three different locations, at each end of the beam and in the middle. See Figure 4. When measuring the width of the beam the flanges were included. The measurement was done with a Vernier caliper. All experiments were repeated three times using the mean measurement for analysis.

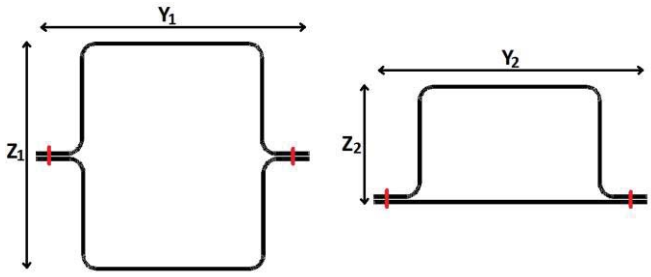

Figure 4 Measurements of welding distortions. Y_1, Z_1, Y_2 and Z_2 were noted for three positions on the beam; in both ends and in the middle of the beam.

3. EXPERIMENTAL RESULTS

3.1 Joint quality

During welding three different welding speeds were used. Representative cross-sections from these can be seen in Figure 5. For welding speed 1.5 m/min (left) the molten material has sunk in the cross-section (commonly known as sagging). Welding speed 3.5 m/min (middle) shows a quite common look of a laser welded thin sheet material. Welding speed 7.5 m/min (right) shows a partially penetrated weld. In conclusion, the results shows that decreased welding speed increases metallurgical impact and may cause weld discontinuities. Consequently, increased welding speed reduces metallurgical impact but will also reduce penetration depth, which may lead to insufficient joint strength.

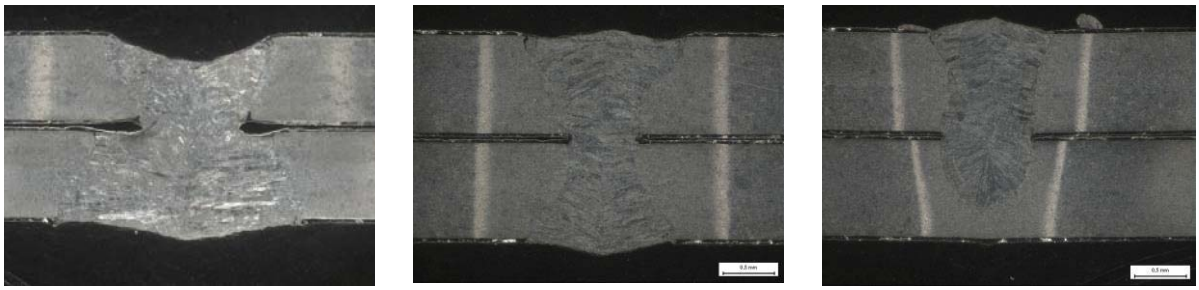

Figure 5 Cross sections of samples welded with travel speed 1.5 m/min (left), 3.5 m/min (middle) and 7.5 m/min respectively.

The rapid cooling from the laser welding process results in fully martensitic structure of the weld. After welding the material rapidly cools resulting in quenching times faster than for diffusion to occur in larger extent. This results in locking of a microstructure which equals to hard martensite (Zhao et al. 2013).

3.2 Distortions

In general, two different characteristic distortion modes occurred for the two geometries welded, see Figure 6. The single hat beam suffered from transverse shrinkage of the gap between the “legs” of the profile. This resulted in a small height change at the ends of the beam. The reason for the height change specifically at the ends is that the built in heat from the process increases along the flange. Something that also was noted was an occasionally low weld quality between the clamps. In these areas the profile has risen from the flat sheet giving a gap resulting in cutting with the laser process.

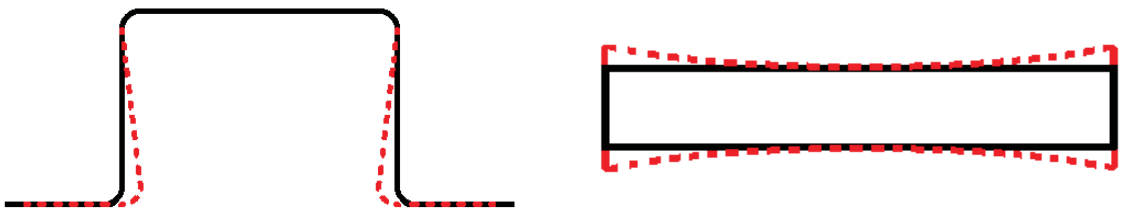

Figure 6 Dominant geometrical distortions occurring after welding for single hat (left) and double hat (right).

The double hat beam suffered from larger distortions than the single hat beam. In this case the geometrical change was in the transverse direction with a hourglass looking shape. Due to the geometrical symmetry of the beam before welding the distortion did not result in a longitudinal bending mode as for single hat, rather

expansion of the cross-section width.

In Figure 7 the measured values of the distortions can be seen. An average value of three repetitions is shown. The results show overall low scatter. For the single hat beam the distortion were small, with a maximum value of around 1.0 mm. For double hat beam the distortions were several magnitudes larger, with maximum around 8.0 mm. For the double hat beam it was clear that a higher heat input resulted in a larger distortion. The results show the effect of the plane sheet of the single hat geometry which increases the stiffness of the geometry, and reduces distortions.

In conclusion, the results show that welding speed significantly affects magnitudes of distortions in the double hat geometry. In addition, in the single hat geometry the distortions are generally smaller compared to the double hat geometry. Thus, the results suggest that welding distortions may be mitigated by advantageous design of structures or optimized process parameters.

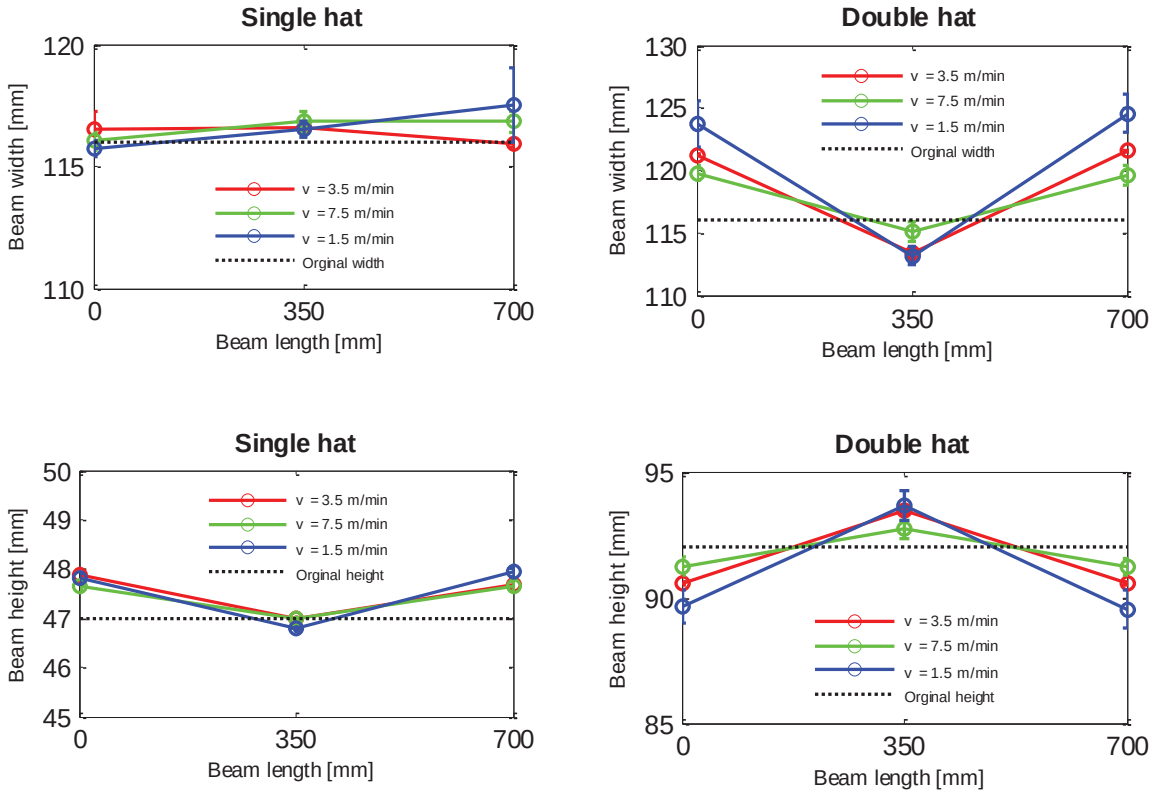

Figure 7 Remaining deformation from welding in both single and double hat geometry. The distortions (height and width) are measured by a Vernier caliper at the edges and in the middle of the beam.

4. SIMULATION TECHNIQUES

An FE model was generated and simulations were performed using ESI Group's Weld Planner. The model consists of quadrilateral shell elements (type: Q4γ) connected with 6-DOF spring elements at the weld line to connect the upper and bottom sheets in the overlap weld, see Figure 8.

In order to simplify the simulation and reduce computation times, laser heat source is modeled as a negative temperature gradient at the region near the weld. Previous researchers have suggested that the temperature gradient should be imposed at the plasticized zone near the weld (Camilleri, 2006). However, as the plasticized zone is difficult to obtain, it is assumed that the plasticized zone is twice as wide as the weld, as recommended by ESI (ESI Group, 2013).

The weld width was obtained from metallographic sections and measurement at the mid-thickness of the sheets from the 3.5 m/min weld results. Figure 9 illustrates the weld sizes at the mid-thickness of the double and single hat geometries. The temperature gradient was imposed at an area twice the size of the weld width in the transverse direction assuming the plasticized zone.

The clamping is modeled by constraining the displacement in all directions to zero at the nodes near the clamps. After the temperature gradient has been imposed the boundary conditions of the clamps are released as in the experimental procedure. The simulations are performed step-wise, as described in Table 3, to model the welding and unclamping. In the final step a boundary condition, which hinders downward displacement of the bottom flange was imposed. This step models the beam resting on the fixture after unclamping.

Table 3 Loads and boundary conditions of finite element model computation steps

Computation step	1	2	3	4	5	6	7
Temperature gradient	1st weld	2nd weld	-	-	-	-	-
Locked boundary conditions	All	All	H1-H4 V1-V4	H1-H3 V1-V3	H1-H2 V1-V2	H1 V1	-

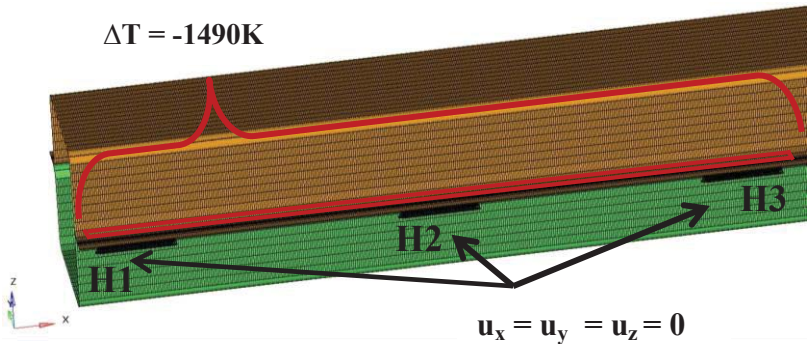

Figure 8 Part of FE model

The material model is defined by the elastic parameters (E = 210 GPa, v = 0.3), yield strength (σ_Y = 1143 MPa) and a plastic flow curve ($\sigma_{pl} = 769\varepsilon^{0.26}$) and the thermal expansion coefficient (α = 1.2e-5 K^{-1}). The temperature gradient is set to ΔT = 1490 K, by defining the solidus temperature as 1783 K and assuming an ambient temperature of 293 K.

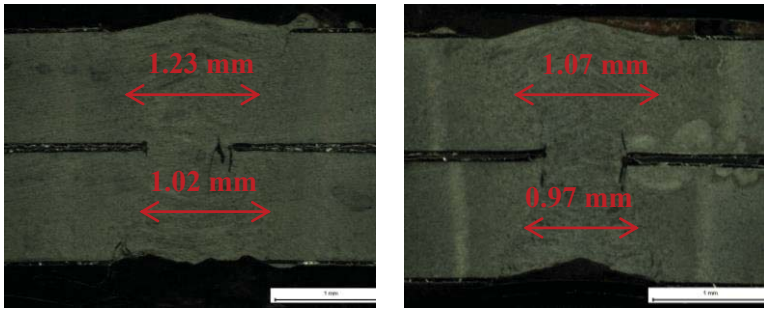

Figure 9 Cross-sections of 3.5 m/min welds of double hat (left) and single hat geometry (right).

5. SIMULATION RESULTS

After the final simulation step a displacement field is generated, which predicts the geometrical distortions due to welding and unclamping. The simulations were completed in approximately 80 minutes, which is significantly less compared to an equivalent transient simulation. Figure 10 shows the transverse shrinkage of the cross-section and the transverse shrinkage along the beam along for the two geometries. As seen, the simulations capture the shape of the distortions of the beam. The temperature gradient causes narrowing of the mid-part of the beam and the expansion of the end parts. Consequently, the mid-part is expanded in the vertical direction and the end parts are contracted vertically. The simulations also capture that the double hat geometry experiences greater distortions compared to the single hat geometry due to the stiffness of the flat sheet, which hinders transverse shrinkage.

In conclusion, the simulations show generally good agreement with experiments. They show that a simplified shell model, which relies on ambient temperature material data, can describe the general behavior of laser beam welding distortions. The results indicate that the extension of the temperature gradient can be approximated by twice the weld width to show promising results.

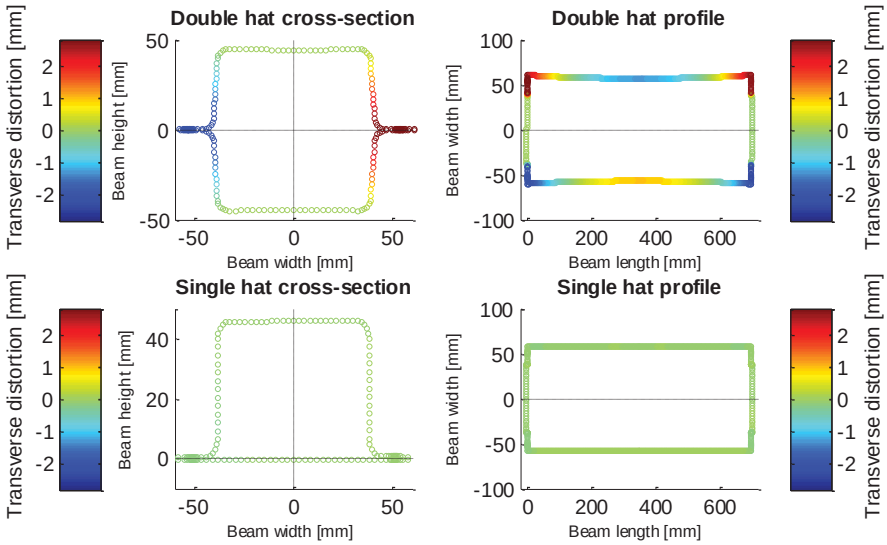

Figure 10 Results of welding distortions from FE model.

6. DISCUSSION

In the present study distortions due to laser welding of UHSS hat profiles were analyzed. The experiments were performed to simulate laser welding of flanges at A-pillar and B-pillar structures, a common application in automotive design. The two chosen geometries gave two different dominant distortion modes.

In order to analyze the distortions accurately and effectively, the experiments were performed in idealized laboratory conditions. While the results give relevant understanding of the laser welding process, in assembly production other factors affect the process which should be taken into account for industrial implementation.

Firstly, the geometries are simplified compared to actual pillars. Therefore more complex distortions or combination of distortion modes may occur in actual A- and B-pillars. Secondly, the present study uses highly controlled and accurate clamping equipment. However, in actual production more economical clamping equipment is commonly used. A relevant continuation of the present work is to investigate more production-like clamping conditions such as RSW tack welds in combination with pressure wheels and their effect on weld quality and distortions.

As presented above, a higher welding speed resulted in lower distortions and nearly maintained weld width at the interface. However, the penetration depth was also lower and the fusion zone did not reach the root of the weld. Thus, such welds cannot be evaluated visually to confirm joint quality. As no effective non-destructive test method for large scale productions exists, the weld parameters are not suitable for production welding. It is of interest to find alternative methods for confirming weld quality of non-fully penetrated welds to use process parameters to reduce welding distortions.

The distortion modes that occur are resulting in an asymmetrical shape along the length of the beam. For single hat beams the transverse shrinking results in bending of the beam. The magnitude of bending is quite small hence the flat sheet is preventing the distortion to accelerate. As seen in the double hat beam both profiles will deform in transverse direction resulting in an hourglass shape. In this case nothing is limiting the distortion resulting in large shape changes up to 8.0 mm. Tolerances of 8.0 mm distortions are excessive for large scale automotive production. If considering the location of the distortion, this is most likely depending on built in heat along the sequence. The longer the weld is, more distortions will occur. From a production view, this could probably be controlled by stitching if strength and fatigue criteria still are fulfilled.

An FE model was presented which relies on simplifications supported by certain assumptions of the welding process in order to reduce computation times and input data requirements. The geometrical simplification through shell element modeling and the heat source simplification through a discrete temperature gradient will not fully describe the physics of the welding process. For example, through thickness variations of temperature and metallurgical transformations are not captured by the model.

Previous research of simplified models of welding distortions, investigated other welding methods, sheet materials and joint configurations. As the previous investigations, the present study shows that the simplified

simulations can quantitatively predict and show the distortional behavior of the structure due to welding. The simulations are also completed in a reasonable time span for industrial implementation for welding engineering work. For a full understanding of the limitations of the simplified approach for a specific case, a full transient analysis should be performed and compared to the simplified results.

Welding distortions are something that needs to be controlled and understood. Within the automotive industry a shape change of 8.0 mm after welding would result in expensive and complicated additional operations. Distortions could therefore be a stopper for the increased use of laser welding of UHSS. Future work needs to include additional parameter variation, more complex geometries that are similar to used components, as well as understanding of how the distortions occur during the welding process.

7. CONCLUSIONS

From this study the following conclusions can be drawn:

- The trials were performed to simulate laser welding of flanges at A-pillar and B-pillar structures. Two chosen geometries gave two different distortion modes. The geometries are simplified and therefore more complex distortions may occur in actual A- and B-pillars.
- Distortion modes occurring was mainly bending and transverse expansion. The single hat beam suffered from longitudinal bending due to its asymmetric geometry. The double hat suffered from transverse expansion resulting in an hourglass shape of the beam. The maximum single hat distortion was around 1.0 mm in comparison with original geometry while the maximum double hat distortion reaches 8.0 mm. For both geometries the largest deformation occurred in the two ends of the beam and the deformation increased with increased heat input.
- A simplified FE model with shell elements and a simplified heat source formulation was developed to model welding distortions. The results show that the simplified model can be used to assess dominant distortions modes of laser welded beam structures after welding and unclamping. The simulations were completed in a reasonable time for industrial implementation.

8. ACKNOWLEDEMENTS

The present research was financed by the Swedish Governement Agnecy VINNOVA within the Vehicle research programme FFI under the contract LASERLIGHT which is gratefully acknowledged. Gratitude is also given to the project committee consisting of Anders Ohlsson (SSAB Group), Janko Banik (ThyssenKrupp Steel) and Håkan Sundberg (Volvo Trucks Corporation) as well as the technicians at Volvo Cars, Esa Laurila and Glenn Hopkins.

REFERENCES

Arcelor Mittal (2010), Hot stamping with USIBOR1500P®, AP&T Advanced hot stamping seminar, Detroit, September 15

Bachorski A., Painter M., Smailes A. och Wahab M. (1999), ”Finite-element prediction of distortion during gas metal arc welding using the shrinkage volume approach,” *Journal of Materials Processing Technology*, Vol. %1 av %292-93, pp. 405-409

Camilleri D., Mollicone P. och Gray T. (2006), ”Alternative simulation techniques for distortion of thin plate due to fillet-welded stiffeners,” *Modelling and Simulation in Materials Science and Engineering*, vol. 14, nr 8, pp. 1307-1327

ESI Group (2013), Weld Planner Manual.

Fahlström K., Larsson JK. (2013), Laser welding of 1900 MPa boron steel, Conference proceedings: NOLAMP 14

Lindgren L.-E. (2001), ”Finite element modeling and simulation of welding part 1: Increased complexity,” *Journal of Thermal Stresses*, vol. 24, nr 2, pp. 141-192

Tikhomirov D., Rietman B., Kose K. och Makkink M. (2005), ”Computing welding distortion: Comparison of different industrially applicable methods,” *Advanced Materials Research*, Vol. %1 av %26-8, pp. 195-202

Verhaeghe G. (1999), Predictive Formulae for Weld Distortion: A Critical Review, Woodhead, 1999.

Zhao Y. Y., Zhang Y.S., Hu W. (2013), “Effect of welding speed, on microstructure, hardness and tensile properties in laser welding of advanced high strength steel”, *Science and Technology of Welding and Joining*, vol.18 no.7

Paper C

C

Minimization of distortions during laser welding of ultra-high strength steel

Karl Fahlström

Oscar Andersson

Urban Todal

Arne Melander

ICALEO
33rd International congress on applications of lasers & electro-optics
San Diego, CA USA, October 2014

MINIMIZATION OF DISTORTIONS DURING LASER WELDING OF ULTRA HIGH STRENGTH STEEL

Karl Fahlström[12], Oscar Andersson[34], Urban Todal[3], Arne Melander[14]

[1] Swerea KIMAB, Joining Technology, Kista, Sweden
[2] University West, Engineering Science, Trollhättan, Sweden
[3] Volvo Cars, Torslanda, Sweden
[4] XPRES, KTH Royal Institute of Technology, Stockholm, Sweden

Abstract

Ultra high strength steels are frequently used within the automotive industry for several components. Welding of these components is traditionally done by resistance spot welding, but to get further productivity and increased strength, laser welding has been introduced in the past decades. Fusion welding is known to cause distortions due to built-in stresses in the material. The distortions result in geometrical issues during assembly which become the origin of low joint quality due to gaps and misfits.

U-beam structures of boron steel simulating B-pillars have been welded with laser along the flanges. Welding parameters and clamping have been varied to create different welding sequences and heat input generating a range of distortion levels. The distortions have been recorded dynamically with an optical measurement system during welding. In addition, final distortions have been measured by a digital Vernier caliper. The combined measurements give the possibility to evaluate development, occurrence and magnitude of distortions with high accuracy. Furthermore, section cuts have been analyzed to assess joint geometry and metallurgy.

The results shows that final distortions appear in the range of 0-8 mm. Distortions occur mainly transversely and vertically along the profile. Variations in heat input show clear correlation with the magnitude of distortions and level of joint quality. A higher heat input in general generates a higher level of distortion with the same clamping conditions. Section cuts show that weld width and penetration are significantly affected by welding heat input.
The present study identifies parameters which significantly influence the magnitude and distribution of distortions. Also, effective measures to minimize distortions and maintain or improve joint quality have been proposed.

Finally, transient FE simulations have been presented which show the behavior of the profiles during the welding and unclamping process.

Introduction

Background

Light weight has been in focus for the automotive industry during several years. Numerous variants of high strength steels have been introduced in the car body, making thinner structures possible without renouncing important properties such as strength, stiffness and crashworthiness. Ultra high strength steel (UHSS) is suitable in several applications within the automotive industry such as front and rear bumper beams, door reinforcements, windscreen upright reinforcements, B-pillar reinforcements, floor and roof reinforcements, and roof and dash panel cross members [1].

A common technology for joining these materials is laser welding. Laser welding can be described as a high productivity welding method suitable for UHSS as well as most automotive applications. Laser welding is usually in comparison with resistance spot welding which historically has been the most used method for joining within body-in-white. The method is associated with low heat input but also high cooling rates which strongly affect the material being welded. This normally results in strong and narrow welds [2].

Due to introduction of heat into the material and asymmetrical structures, welding will cause expansion and shrinking to result in unwanted remaining geometry changes in the design. It is necessary to control these distortions and minimize

the residual stresses in the material, or at least, ensure that the design allows them. If not, geometrically important points for assembly can be displaced several millimeters resulting in gaps causing low product quality and risk of costly post-welding repair work [3].

Mathematical modeling and FE simulations of laser beam welding distortions have been researched for the past decades. Works have been published, investigating modeling of laser welds in steel in butt joint [4] , T-joint [5] and lap joint [6] configurations. However, in the literature no detailed models of laser welding of UHSS have been found.

Due to the very high temperature gradients and non-linearity of welding computations, FE simulations have been extremely time-consuming. To reduce computation times adaptive meshing [7], 2D shell element modeling [8], simplified heat source formulations and material models [9] have been suggested.

The present work uses a transient thermo-metallurgical-mechanical solid element model of a reduced geometry to analyze welding deformations due to a moving heat source. Temperature dependent thermal, mechanical and metallurgical data have been generated for the UHSS material.

Aim of Paper

The aim of this paper is to investigate where, when, and in what magnitude and form, distortions occur while laser welding press-hardened boron steel. Welding will be done on hat profile beams simulating A-pillars and B-pillars. Also, FE simulations will be performed to further analyze welding distortions.

Experimental procedure

Material

In the present study martensitic presshardened MBW 1500P with AlSi coating (+AS) was used, delivered from ThyssenKrupp Steel. The steel was hot formed into a U-beam-geometry which in combination with a flat sheet could be altered into two geometries generating two different distortion modes, see Figure 1. One beam should give possibility to asymmetric deformation when joining a hat-profile with a flat sheet (hereafter named “single hat”) of MBW1500P, and the other symmetric deformation along the neutral plane of the geometry when joining two hat-profiles (hereafter named “double hat”). The two cases were chosen as simplified models to simulate A- and B-pillar. The thickness of the material was 1.0 mm with a beam length of 700 mm.

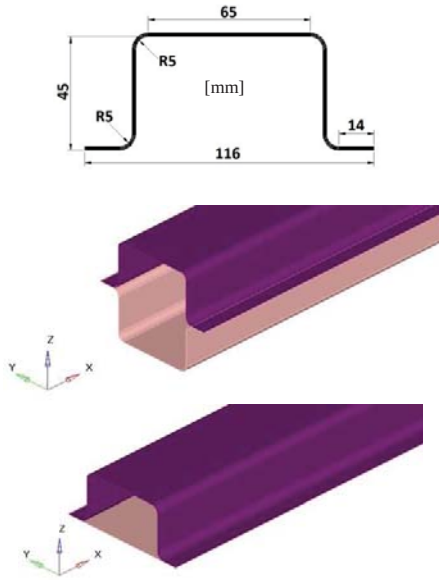

Figure 1 Cross-section data (top) and single hat (bottom) and double hat (middle) geometries.

Fixture And Welding Sequence

The beam was mounted in a robust fixture, shown in Figure 2. The fixture holds the flanges with five 40 mm wide clamps evenly distributed on each flange, using pneumatics. The clamping force was set individually for each clamp. The welding was done at the center of the flange in opposite directions for the two sides, as illustrated by the red arrows in Figure 2. The clamps covered 3 mm of the flange perpendicular to the longer edge. The full sequence consisted of welding, cooling for three minutes, and then unclamping with 10 seconds between unclamping each opposite pair of clamps starting from one end. The last clamping pair (H1 + V1) was unclamped after 30 seconds instead of 10 seconds. The welding and unclamping sequence is described in Table 1.

Table 1 Describing the welding and unclamping sequence.

Welding during 11/24/55 sec depending on welding speed	Cooling during 180 sec	Unclamping pair H5 + V5	Unclamping pair H4 + V4 after 10 sec	Unclamping pair H3 + V3 after 10 sec	Unclamping pair H2 + V2 after 10 sec	Unclamping pair H1 + V1 after 30 sec

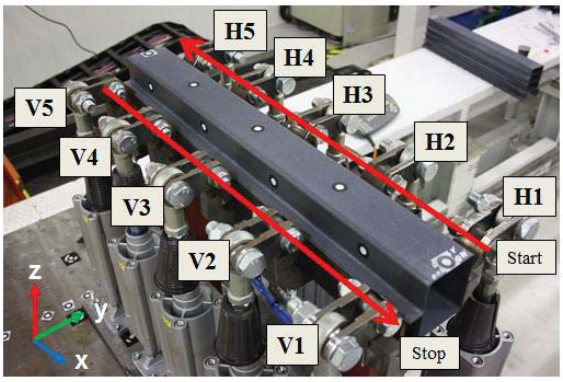

Figure 2 Welding fixture with beam, welding directions, measurement points and clamping

The pneumatic clamping was set on 4 bars to ensure sufficient force holding the beams. If choosing a lower clamping force the beams would distort and create a gap at the faying surface resulting in cutting effects from the laser beam.

The welding was done with a HL4006D Nd:YAG laser from Trumpf with Permanova optics (200/200). 4kW power was used with a 0.6 mm spot diameter with focus position on the top surface of the material. The welding speed was set at 1.5, 3.5 and 7.5 m/min. The optics was placed perpendicular to the sheet surface and welding direction. Three scenarios were created only varying the welding speed to create different heat inputs to the material.

Measurement Of Distortions

After the welding sequence, cooling and unclamping the beam geometry was measured. The total height and width of the beam was measured at three different locations, at each end of the beam and in the middle, see Figure 3. When measuring the width of the beam the flanges was included. The measurement was done with a Vernier caliper.

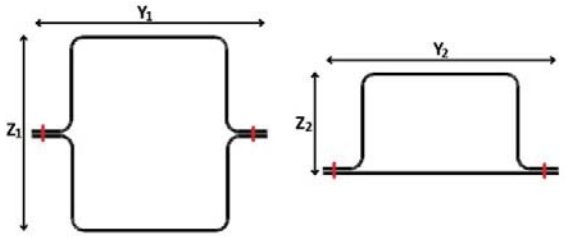

Figure 3 How the distortion measurements were performed. Y1, Z1, Y2 and Z2 were noted for three positions on the beam; in both ends and in the middle of the beam

For more advanced measurement of distortions an optic measurement technology Move Inspect by Aicon was used. The system consist of three cameras placed at a distance of approximately 2 m from the beam. The system recognizes measurement points (shown in Figure 4) placed on the beam, and record the position with x-, y-, and z- coordinates at a frequency of 2 Hz. The recording was done during the whole sequence.

In total 9 measurement points were placed on the beam. 5 was evenly distributed on the top surface of the beam and 4 on one of the sides of the upper beam, represented by the white circles on the beam surface seen in Figure 2.

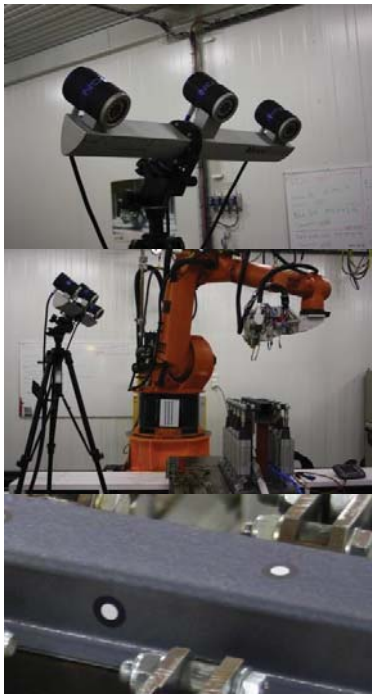

Figure 4 The camera (top), set-up (middle) and measurement points (bottom) used for measurement of distortions during welding.

Experimental Results

Joint Quality

During welding three different welding speeds were used. Representable cross-sections from these can be seen in Figure 6. Welding speed 1.5 m/min (left) show that the molten material has sunk in the cross-section (sagging). Welding speed 3.5 m/min (middle) show a quite common look of a laser welded thin sheet material with a typical hourglass shaped weldment. Welding speed of 7.5 m/min (right) show a partially penetrated weld. For all welding speeds the rapid cooling after laser welding results in fully martensitic structure of the weld. The cooling corresponds to quenching times faster than for diffusion to occur in larger extent. This results in locking of a microstructure which equals to hard martensite. Ferrite structure occurs, although outside the weld, as an annealed area with softer material [10].

Occurrence Of Distortions

The sequence including welding, cooling and unclamping was recorded with optical measurements. The total welding time differed since different welding speeds was used. The optical measuring equipment recorded distortions in all measurement points during welding After welding the distortions retracted to approximately initial value. This is due to strong clamping. During cooling very low distorions were recorded compared to during welding. When the unclamping began stepwise increase of distortions arised resulting in final distorted geometry. A schematic figure of the full sequence is illustrated in Figure 5.

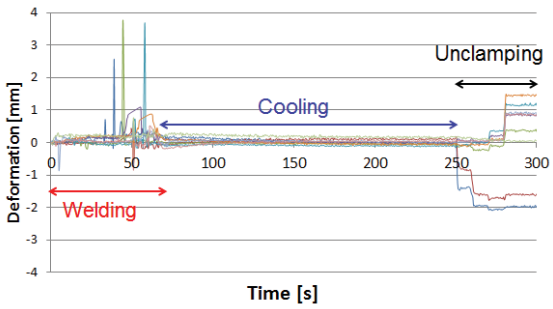

Figure 5 Schematic figure of the distortions occurring during welding, cooling and unclamping. The different curves represent different measurement points

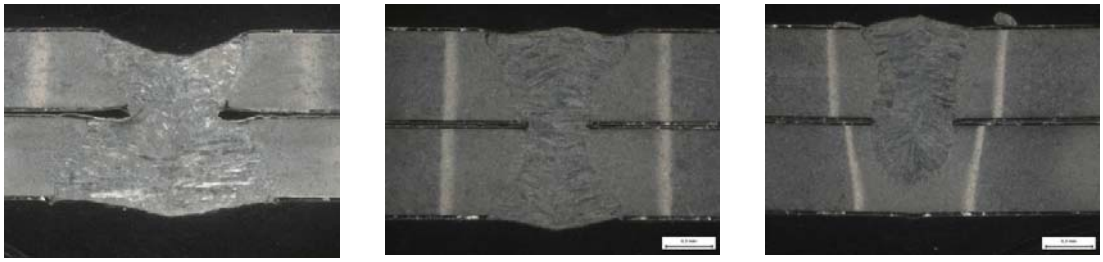

Figure 6 Cross sections of welds with travel speed 1.5 m/min (left), 3.5 m/min (center) and 7.5 m/min respectively

Geometry Change Due To Distortions

In general, two different characteristic distortion modes occurred for the two geometries welded, see Figure 7. The single hat beam suffered from transverse shrinkage of the gap between the "legs" of the profile. This resulted in a small height change at the ends of the beam. The reason for the height change specifically at the ends is that the built in heat from the process increases along the flange. Something that also was noted was an occationally low weld quality between the clamps. In these areas the profile has risen from the flat sheet giving a gap resulting in cutting with the laser process.

The double hat beam suffered from larger distortions than the single hat beam. This is due to that the flat sheet's high stiffness hindered transverse distortion in the single hat geometry. For double hat, the geometrical change was in the transverse direction with a hourglass looking shape. Due to the geometrical symmetry of the beam before welding the distortion did not result in a longitudinal bending mode as for single hat, rather expansion of the cross-section width. The flat sheet in the single hat gave a lower longitudinal bending stiffness compared to the double hat geometry.

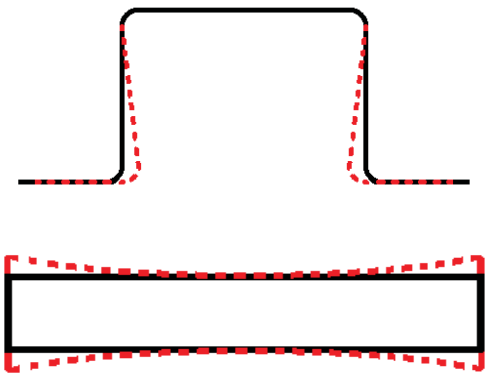

Figure 7 Dominant geometrical distortions occurring after welding for single hat (top) and double hat (bottom). Black line is showing ideal initial shape

Measurements of final distortions with the optical measurements technique were carried out for double hat beam. In Figure 8 distortions in y-direction (transverse) as well as z-direction (vertical) can be seen. The maximum remaining absolute distortions are in the range of 2 mm for vertical deformation and 1.5 mm for transverse deformation. Note that the last clamping pair (H1+V1) was still mounted during recording of these values. Measurement points (1-5 for z-coordinates and 1-4 for y-coordinates) were positioned evenly distributed over the length of the beam.

The final state of the distortion was also measured with Vernier caliper. The results can be seen in Figure 9. For the single hat beam the distortion were small, with a maximum value of around 1.0 mm. For double hat beam the distortions were several magnitudes larger, with maximum around 8.0 mm. For the double hat beam it was clear that a higher heat input resulted in a larger distortion. The partially penetrated welds have un-molten material in the root of the weld that prevents distortions.

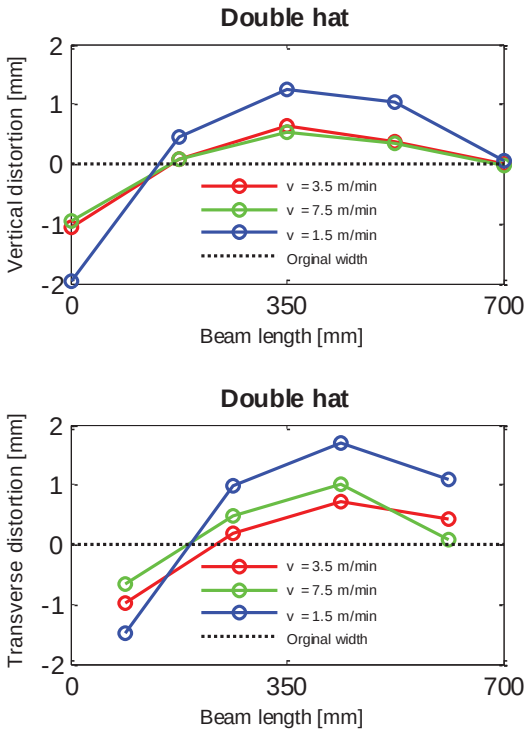

Figure 8 The distortions remaining after unclamping all clamps but H1+V1. The upper figure shows the z-distortion (vertical) and the lower figure shows the y-distortion (transverse)

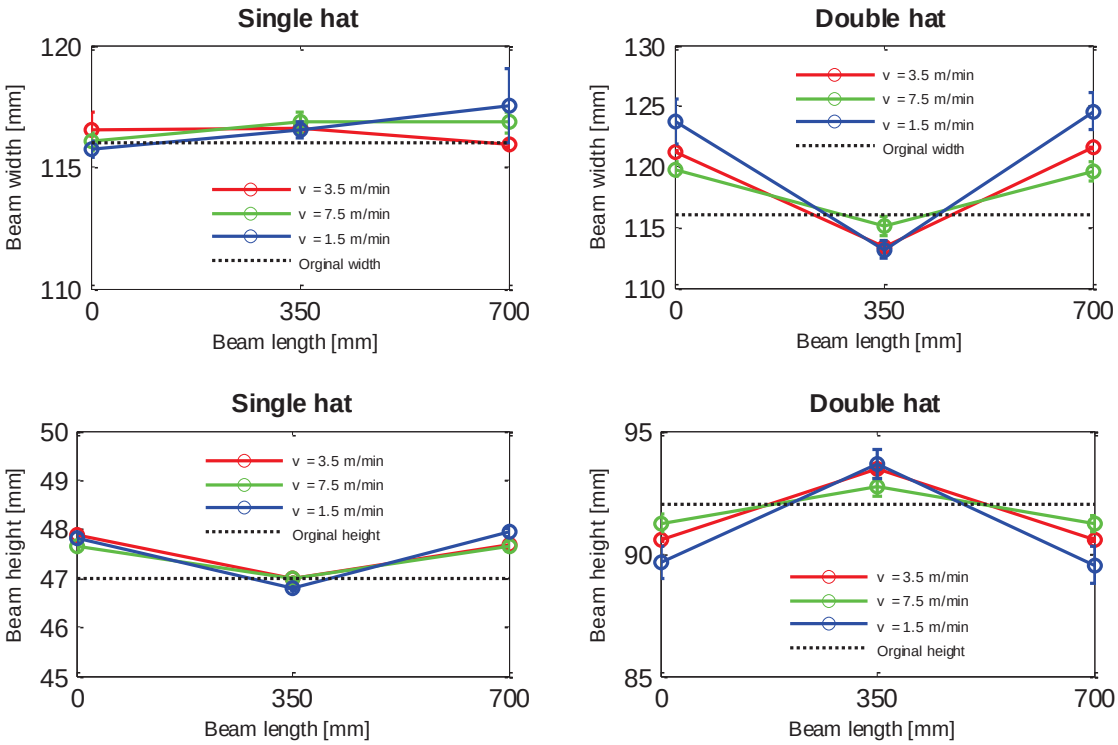

Figure 9 The remaining deformation from welding in both single and double hat geometry. The distortions (height and width) are measured by Vernier caliper at the edges and in the middle of the beam

In conclusion, the results show that welding speed significantly affects magnitudes of distortions in the double hat geometry. In addition, for the single hat geometry the distortions are generally smaller compared to the double hat geometry.

Finite Element Model

A thermo-metallurgical-mechanical computational model was developed using ESI'S SYSWELD code. An uncoupled procedure was used, where a thermal analysis is performed to compute temperature histories which are used for a mechanical analysis in a subsequent step to obtain the displacement field. In order to reduce computation times, only a characteristic sub-geometry was analyzed, namely a section around one clamp - a distance of 160 mm, as shown in Figure 10.

Thermal Analysis

The thermal problem is modeled by the general heat conduction equation as shown in equation (1).

$$_{p}\rho\frac{\partial T}{\partial t} = \lambda\nabla^2\frac{\partial T}{\partial u} + Q \qquad (1)$$

where $c_{p,}$ ρ and λ are the specific heat, density and heat conductance, respectively and Q is the total internal heat source intensity.

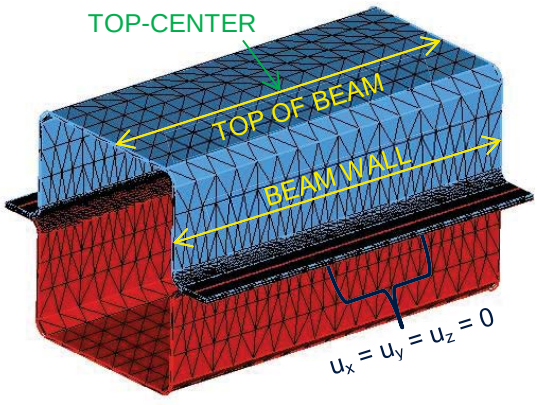

Figure 10 Finite element model

The thermal material data can be seen in Figure 11. The density and specific heat data were obtained by THERMOCALC [11] computations and the conductivity was obtained through IDS [12] computations.

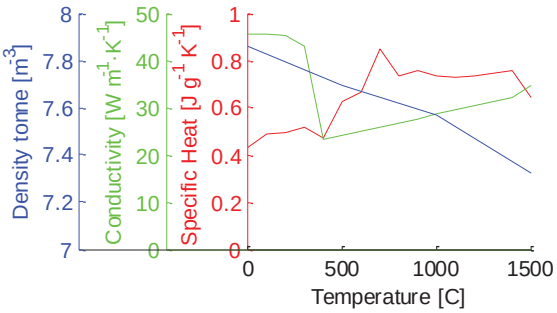

Figure 11 Thermal material data

The laser weld heat source is modeled by conical Gaussian conductive model to describe the heat input of the laser beam process, formulated as in Equation (2).

$$Q_{keyhole} = \frac{2\eta Q_{beam}}{\pi h r_{beam}^2} e^{\left(1-\frac{r}{r_{beam}}\right)} \left(1-\frac{z}{h}\right) \qquad (2)$$

where η is the beam efficiency (assumed to be 70% [4]), Q_{beam} is the power output of the laser beam (4 kW), h is the total thickness of the sheets, assuming full penetration of the weld (2 mm), r_{beam} is the beam radius at the focus position (0.3 mm) and r and z are radial and depth coordinates, respectively. The moving heat source was applied at 3.5 m min^{-1} at in a horse shoe pattern. The welding process spans over the first 5.49 s of the simulation.

The heat losses from the sheet surface are modeled by radiation through Stefan-Boltzmann's law (using Stefan-Boltzmann constant, σ = 5.67e-8 W m^{-2} K^{-4} and surface emissivity, ε = 0.8) and by convection through a surface convection coefficient of 25 W m^{-2}.

Mechanical Analysis

The temperature history from the thermal analysis is passed on to a mechanical analysis, decomposed into four strain components as shown below.

$$\varepsilon = \varepsilon_{el} + \varepsilon_{pl} + \varepsilon_{th} + \varepsilon_{met} \qquad (3)$$

The first term on the right hand side corresponds to the elastic strain which is modeled temperature dependent Young's modulus and Poisson's ratio. The second term corresponds to the plastic strain, modeled by a temperature dependent von Mises yield limit and isotropic hardening model. The mechanical data, shown in Figure 12 and Figure 13, were obtained by tensile tests. A Poisson's ratio of 0.33 was assumed. The third term corresponds to the thermal strains modeled by a coefficient of thermal expansion obtained by dilatometer tests as 13.6 10^{-6} K^{-1}.

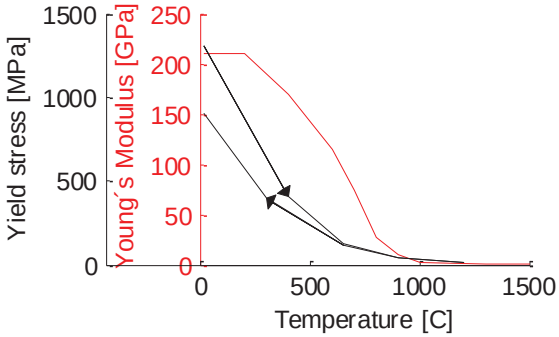

Figure 12 Mechanical material data

The fourth term corresponds to martensitic transformation strains, modeled by the Koistinen-Marburger [13] (Ms = 415C, n = 0.142) and Leblond models [14].

The clamping was modeled by locking all displacements at the nodes located at the clamp, as indicated in Figure 10, for the first 30 s of the simulation. After unclamping the flange, a contact condition is imposed, which hinders the flange edges to move in a downward direction, which represent the fixture the beam is resting on.

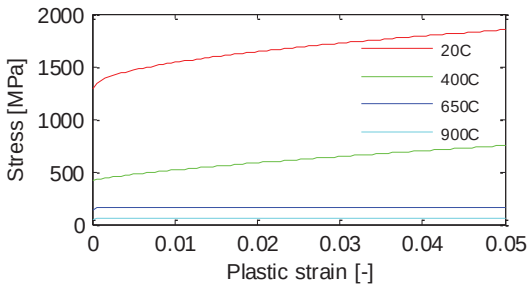

Figure 13 Plastic deformation model

Simulation Results

The FE model generates a displacement field which describes the distortions during welding process. A number of locations of interest have been selected for analysis, as indicated in Figure 10.

In Figure 14, the transverse distortions along the beam wall are shown. The results show the hour-glass shape of the beam. However, the simulations show that during the welding process inverted distortions occur. Subsequently, after cooling, the distortions are reversed and further augmented after unclamping.

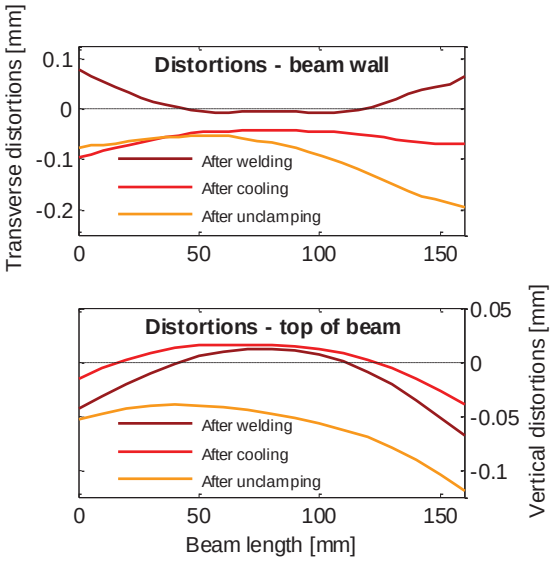

Figure 14 Distortions results of FE model

In Figure 14 the vertical distortions along the top of the beam are shown. The general shape and distribution of the distortions are accurately modeled showing a relative positive distortion at the center of the structure and relative negative displacement at the edges. The results also show a global distortion after unclamping while relative distortions are nearly intact.

Figure 15 shows the transient displacements at the center point at the top of the beam. The results show rapid distortions during the welding sequence and a stabilization of distortions during the cooling process. After unclamping a clear change in distortions take place. However, as noticed in Figure 14, the vertical unclamping distortions are globally distributed.

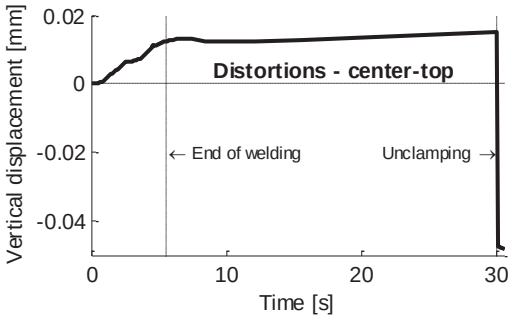

Figure 15 Transient distortion results

Discussion

In the present study distortions due to laser welding of UHSS hat profiles were analyzed. The experiments were performed to simulate laser welding of flanges at A-pillar and B-pillar structures, a common application in automotive design. The two chosen geometries gave two different dominant distortion modes.

In order to analyze the distortions accurately and effectively, the experiments were performed in idealized laboratory conditions. The geometries are simplified compared to actual pillars. Therefore more complex distortions or combination of distortion modes may occur in actual A- and B-pillars.

As presented above, a higher welding speed resulted in lower distortions. However, the penetration depth was also lower and the fusion zone did not reach the root of the weld. Thus, such welds cannot be evaluated visually to confirm joint quality. As no effective non-destructive test method for large scale productions exists, the weld parameters are not suitable for production welding. It is of interest to find alternative methods for confirming weld quality of non-fully penetrated welds to use process parameters to reduce welding distortions.

The distortion modes that occur are resulting in an asymmetrical shape along the length of the beam. For single hat beams the transverse shrinking results in bending of the beam. The magnitude of longitudinal bending is minor since the flat sheet is preventing the distortion to augment. As seen in the double hat beam both profiles will deform in transverse direction resulting in an hourglass shape. In this case nothing is

limiting the distortion resulting in large shape changes up to 8.0 mm measured with Vernier caliper. Tolerances of 8.0 mm distortions are excessive for large scale automotive production. If considering the location of the distortion, this is most likely depending on built in heat along the sequence. The longer the weld is, the more distortions will occur. From a production view, this could probably be controlled by intermittent welding if strength and fatigue criteria still are fulfilled.

The distortions are expected to increase when the last clamping is removed, hence the difference from optical measurements compared to Vernier caliper-measurements. If assuming that measurements done with the optical equipment only demonstrate geometry changes from half of the profile since measurement points only is placed on the top side of the beam, the results correlate even more with measurements done with Vernier caliper. This would give transverse distortions in the magnitude of 4 mm compared to 8.0 mm. This comparison shows the significant effect of the final unclamping on the magnitude of distortions.

Regarding the geometrically reduced FE model it shows that it can describe the history and distribution of temperatures and distribution and development of distortions due to welding and unclamping. For a full qualitative assessment of distortions a geometrically complete model is, however, preferred.

The welding distortions are something that needs to be controlled and understood. Within the automotive industry a shape change of 8.0 mm after welding would result in expensive and complicated additional operations. If not control, distortions could therefore be a stopper for the increased use of laser welding of UHSS. Future work needs to include additional parameter variation, more complex geometries that are similar to used components, as well as further understanding of why the distortions occur during the welding process. Thus, the results suggest that welding distortions may be mitigated by advantageous design of structures or optimized process parameters.

Conclusions

From this study the following conclusions can be drawn:

- The trials were performed to simulate laser welding of flanges at A-pillar and B-pillar structures. Two chosen geometries gave two different distortion modes. The geometries are simplified and therefore more complex distortions will occur in actual A- and B-pillars.
- Distortion modes occurring was mainly bending and transverse expansion. The single hat beam suffered from longitudinal bending due to its asymmetric geometry. The double hat suffered from transverse expansion resulting in an hourglass shape of the beam. The maximum single hat distortion was around 1.0 mm in comparison with original geometry while the maximum double hat distortion reaches 8.0 mm.
- Measurements with optical measurement technique in comparison with Vernier caliper show great potential for usage during the welding sequence for further understanding. Distortions do occur, but retract during welding. During cooling the material is rather fixed. After welding during the unclamping the distortions were arising stepwise with each clamp.
- The final distortions do correlate with measurements from Vernier caliper and optical measurements.
- A FE sub-model of the structure was generated and transiently analyzed with a thermo-metallurgical-mechanical material model. The simulation results show that the model can describe the general behavior of the complete structure during welding, cooling and unclamping. However, for a complete qualitative comparison and prediction of welding distortions a full geometrical model may be analyzed.

Acknowledgements

The present research was financed by the Swedish Governement Agency VINNOVA within the Vehicle research programme FFI under the contract LASERLIGHT which is gratefully acknowledged. Gratitude is also given to the project committee consisting of Anders Ohlsson (SSAB Group), Janko Banik (ThyssenKrupp Steel) and Håkan Sundberg (Volvo Trucks Corporation) as well as the technicians at Volvo Cars, Esa Laurila and Glen Hopkins. Also a special thanks to Lars-Erik Svensson and Leif Karlsson at University West.

References

[1] Arcelor Mittal, "Hot stamping with USIBOR1500P," in *AP&T Advanced hot stamping seminar*, Detroit, 2010.

[2] K. Fahlström and J. Larsson, "Laser welding of 1900 MPa boron steel," in *NOLAMP14*, Gothenburg, 2013.

[3] M. Geiger, "Flexible Straightening of Car Body Shells by Laser Forming," SAE Technical Paper 930279, 1993.

[4] S. Tsirkas, P. Papanikos and T. Kermanidis, "Numerical simulation of the laser welding process in butt-joint specimens," *J. Mater. Process. Technol.*, vol. 134(1), pp. 59-69, 2003.

[5] C. Darcourt, J. Roelandt, M. Rachik, D. Deloison and B. Journet, "Thermomechanical analysis applied to the laser beam welding simulation of aeronautical structures," *J. Phys. IV*, vol. 120, pp. 785-792, 2004.

[6] J. Ma, F. Kong and R. Kovacevic, "Finite-element thermal analysis of laser welding of galvanized high-strength steel in a zero-gap lap joint configuration and its experimental verification," *Mater. Des.*, vol. 36, p. 348–358, 2012.

[7] H. Runnemalm and S. Hyun, "Three-dimensional welding analysis using an adaptive mesh scheme," *Comput. Method. Appl. M.*, vol. 189(2), pp. 515-523, 2000.

[8] L.-E. Lindgren and L. Karlsson, "Deformations and stresses in welding of shell structures," *Int. J.Numer. Meth. Eng.*, vol. 25(2), p. 635–655, 1988.

[9] A. Bachorski, M. Painter, A. Smailes and M. Wahab, "Finite-element prediction of distortion during gas metal arc welding using the shrinkage volume approach," *J. Mater. Process. Technol.*, vol. 93, pp. 405-409, 1999.

[10] Y. Y. Zhao, Y. Zhang and W. Hu, "Effect of welding speed on microstructure, hardness and tensile properties in laser welding of advanced high strength steel," *Sci. Technol. Weld. Joi.*, vol. 18(7), pp. 581-590, 2013.

[11] "Thermo-Calc for Windows Version 5 User's Guide June 2008".

[12] J. Miettinen, S. Louhenkilpi, H. Kytönen and J. Laine, "IDS: Thermodynamic-kinetic-empirical tool for modelling of solidification, microstructure and material properties," *Math. Comput. Simulat.*, vol. 80(7), pp. 1536-1550, 2010.

[13] D. Koistinen and R. Marburger, "A general equation prescribing the extent of the austenite-martensite transformation in pure iron-carbone alloys and plain carbon steels," *Act.A Metall. Mater.*, vol. 7, pp. 59-60, 1959.

[14] J. Leblond, "Mathematical modelling of transformation plasticity in steels II. Coupling with strain hardening phenomena," *Int. J. Plasticity*, vol. 5, pp. 573-591, 1989.

Laser Welding of Boron Steels for Light-Weight Vehicle Applications

In this work new material and joining solutions for light-weight vehicles are investigated. Both laser welding and boron steels has been identified to be promising for the automotive industry. During laser welding of boron steels quality issues such as imperfections, changes in local and global geometry as well as strength reduction can occur. These could be fatal for the construction and the occurrence needs to be minimized.

The study includes laser welding of boron alloyed steels with strengths of 1500 MPa and a recently introduced 1900 MPa grade. Focus has been to investigate weldability and the occurrence of imperfections and distortion. The results show that both conventional and 1900 MPa boron alloyed steel are suitable for laser welding. Results from tests done on U-shaped beams indicate that depending on the geometry and weld heat input distortions from 1 to 8 mm, at a welding length of 700 mm can occur.

ISBN 978-91-87531-04-0